



ELSEVIER

Contents lists available at ScienceDirect

Quaternary Science Reviews

journal homepage: www.elsevier.com/locate/quascirev

Declining discharge of glacier outburst floods through the Holocene in central Patagonia



Gerardo Benito ^{a,*}, Varyl R. Thorndycraft ^b, Alicia Medialdea ^c, Maria J. Machado ^a, Carlos Sancho ^d, Alejandro Dussaillant ^{e,f,g}

^a Department of Geology, National Museum of Natural Sciences (MNCN), CSIC, Serrano 115 bis, 28006, Madrid, Spain

^b Department of Geography, Royal Holloway University of London, Egham TW20 0EX, UK

^c Centro Nacional de Investigación sobre la Evolución Humana, CENIEH, Paseo Sierra de Atapuerca, 3. 09002 Burgos, Spain

^d Departamento de Ciencias de la Tierra, Universidad de Zaragoza, 50009, Zaragoza, Spain

^e Departamento de Ciencias Naturales y Tecnología, Universidad de Aysén, 5951360, Coyhaique, Chile

^f Centro de Investigación en Ecosistemas de la Patagonia, 5950000, Coyhaique, Chile

^g Department of Natural Sciences, Middlesex University, London NW4 4BT, UK

ARTICLE INFO

Article history:

Received 3 September 2020

Received in revised form

11 January 2021

Accepted 13 January 2021

Available online 17 February 2021

Handling Editor: Giovanni Zanchetta

Keywords:

Geomorphology

GLOFs

Palaeohydrology

Palaeosols

South America

ABSTRACT

Glacier outburst floods are a major hazard in glacierized catchments. Global analyses have shown reduced frequency of glacier floods over recent decades but there is limited longer-term data on event magnitude and frequency. Here, we present a Holocene palaeoflood record from the Río Baker (Chilean Patagonia), quantifying the discharge and timing of glacier floods over millennial timescales. A catastrophic flood of 110,000 m³/s (0.11 Sv) occurred at 9.6 ± 0.8 ka, during final stages of the Late Glacial Interglacial Transition, followed by five flood-phases coeval or post-dating Holocene neoglacials. Highest flood frequencies occurred at 4.3–4.4 ka, with 26 floods of minimum discharges of 10,000–11,000 m³/s, and 0.6 ka with 10 floods exceeding 4600–5700 m³/s. The largest modern outburst flood recorded surpassed ~3810 m³/s. Thus glacier flood magnitude declines from the order of 0.1 to 0.01 Sv over the Early to Mid Holocene, and to 0.001 Sv in the instrumental record.

© 2021 The Authors. Published by Elsevier Ltd. This is an open access article under the CC BY-NC-ND license (<http://creativecommons.org/licenses/by-nc-nd/4.0/>).

1. Introduction

Glacier lake outburst floods (GLOFs), the sudden release of water from glacier or moraine-dammed lakes, are important natural hazards due to the sudden release of large volumes of water, often causing greater discharges than conventional floods in the same catchment (Walder and Costa, 1998; Dussaillant et al., 2009; Jacquet et al., 2017). With regards to geomorphic processes, outburst floods can cause significant erosion (Cook et al., 2018) and sediment transport (Snorrason et al., 2002), often contributing to some of the most extreme sediment delivery events globally (Korup, 2012). GLOFs are of particular contemporary interest due to the role of climate change on the magnitude and frequency of

events and therefore societal risk (Carrivick and Tweed, 2016). In a global analysis of GLOFs it was found there was a decrease in flood frequency over recent decades (Carrivick and Tweed, 2016), despite remote sensing studies that show an increase in the number and area of glacial lakes in regions such as Greenland (Carrivick and Quincey, 2014), the Himalaya (Dubey and Goyal, 2020) and Patagonia (Loriaux and Casassa, 2013; Wilson et al., 2018). Focusing only on moraine dam failures, Harrison et al. (2018) note a reduction in floods since the 1970s, but also argue that the greatest frequency of events (1930s–1960s) reflect a lagged response to warming at the end of the Little Ice Age (LIA). Based on their empirical data on the timing of climate forcing followed by lagged glacier recession, lake formation and moraine-dam failure, Harrison et al. (2018) hypothesise increased frequencies of glacier outburst flooding over forthcoming decades.

Missing from these global analyses, however, are sufficient data on flood discharge to infer time-dependent trends in glacier flood magnitude and frequency. Available records typically span a

* Corresponding author.

E-mail addresses: benito@mncn.csic.es (G. Benito), Varyl.Thorndycraft@rhul.ac.uk (V.R. Thorndycraft), alicia.medialdea@cenieh.es (A. Medialdea), csancho@unizar.es (C. Sancho), alejandro.dussaillant@uaysen.cl (A. Dussaillant).

relatively short timeframe, relying on observed events in the historical and instrumental records, with sparse data before the 20th Century (Carrivick and Tweed, 2016). There is, therefore, a need for empirical data on flood magnitude and timing of GLOFs over longer (centennial to millennial) timescales. The Baker valley in central Chilean Patagonia (Fig. 1) provides potential for developing a palaeoflood record spanning the Holocene as demonstrated by: a) the geomorphic evidence for catastrophic and extreme flood landforms along bedrock gorge reaches (Benito and Thorndycraft, 2020); and b) alternating organic and clastic sediments preserved in alluvial floodplain settings (Vandeckerhove et al., 2020).

Herein, we reconstruct a Holocene glacier flood magnitude and frequency record from narrow bedrock reaches of the Río Baker catchment using palaeoflood approaches (Baker and Kochel, 1988; Benito and Thorndycraft, 2005; Carrivick et al., 2013), to evaluate the long-term temporal evolution of GLOF magnitude, and the timing of changing GLOF frequency in relation to regional glacier dynamics. The objectives of the study are to: a) use remotely sensed and field geomorphological mapping to classify flood landforms along the Río Baker; b) analyse flood stratigraphy, preserved by slackwater flood landforms, to determine the number of flood events preserved at a site; c) determine the timing of flood events through radiocarbon and optically stimulated luminescence (OSL) dating; and d) simulate past floods using one-dimensional hydraulic flood modelling to calculate palaeodischarges.

2. Study area

2.1. Río Baker catchment

Our study area is the Río Baker, which drains a transnational catchment of $\sim 29,000 \text{ km}^2$ in central Patagonia (Fig. 1, Dussaillant et al., 2012). The climate is temperate oceanic, according to the Köppen classification, with a high influence of relief on both temperature and precipitation gradients. Precipitation varies from west

to east across the basin with annual values of $\sim 1700 \text{ mm/a}$ at Lago Vargas, near the Pacific coast in the western glaciated catchments, to $\sim 220 \text{ mm/a}$ at Chile Chico (Fig. 1) in the eastern steppe (Dussaillant et al., 2012). The source of the main trunk of the Baker is at Lago Bertrand (Fig. 2), itself fed by Lago General Carrera/Buenos Aires, South America's second largest lake ($\sim 1800 \text{ km}^2$). The major western tributaries of the Río Baker (from north to south, the Nef, Colonia and Ventisquero rivers) drain the eastern ice-shed of the Northern Patagonia Icefield (NPI; Figs. 1 and 2) so are fed by meltwater in the summer, and drain proglacial lakes dammed by Holocene moraines. The eastern tributaries are more varied in their geography. The Chacabuco drains an area of steppe; Río Cochrane is sourced from Lago Cochrane, the second largest lake of the basin (Fig. 1); the Río del Salto drains the Monte San Lorenzo ice-cap and is fed by multiple proglacial lakes; and the Río de los Ñadis drains a region of small glaciers in the southeast of the catchment (Fig. 2).

The geology of the Baker catchment comprises five major zones: 1) the eastern limit of the Baker watershed (Fig. 1), and present Atlantic-Pacific water divide, is a low relief landscape dominated by Quaternary glaciogenic and fluvioglacial deposits (Caldenius, 1932; Mercer, 1976; Douglass et al., 2006; Hein et al., 2010; Bendle et al., 2017b); 2) a belt of N–S mountainous relief ($\sim 72.3^\circ\text{W}$) with Jurassic age acidic volcanic and volcano-sedimentary rocks (De La Cruz et al., 2004; Niemeyer et al., 1984); 3) Palaeozoic basement ($\sim 73^\circ\text{W}$) made of low grade metapelites and greenschist facies (Hervé, 1993); 4) the Cosmelli Basin, an uplifted syncline infilled with Miocene continental molasses (Flint et al., 1994), located between the Lago General Carrera and the Río Chacabuco valley ($\sim 47^\circ\text{S}$ – 72.5°W); and 5) the Patagonian calc-alkaline granite batholith (73 – 74°W) occupying the high relief of the Northern Patagonia Icefield (Fig. 1).

The Baker catchment was almost entirely covered in ice during the local Last Glacial Maximum (Davies et al., 2020). Warming from $\sim 18.1 \text{ ka}$ saw accelerated recession of the NPI outlet lobe (Bendle et al., 2017a) occupying the present-day basin of Lago General

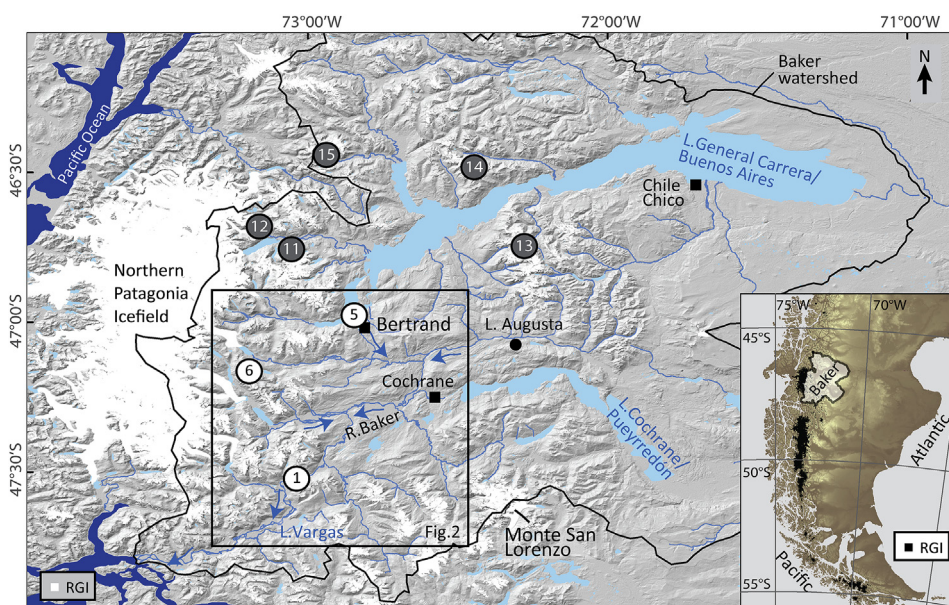


Fig. 1. The Río Baker catchment and location of selected ice-dammed GLOFs (white circles) and moraine-dammed GLOFs (grey circles) (see Table 1 for details). The study reaches are located in the Cochrane region (see Fig. 2). Also shown is the location of the Lago Augusta pollen record (Villa-Martínez et al., 2012). The earliest GLOF event discussed in this paper is the drainage of Palaeolake Chelenko (Site 1, Thorndycraft et al., 2019), which was formed when the General Carrera/Buenos Aires and Cochrane/Puerrredón lakes were unified through the Baker valley (Turner et al., 2005). Inset: Southernmost South America showing the location of the Baker catchment in central Patagonia. Shown on both maps is the Randolph glacier inventory Zone 17 (RGI), which in the main panel shows the Northern Patagonia Icefield and main valley glaciers in the region, including the Monte San Lorenzo ice cap.

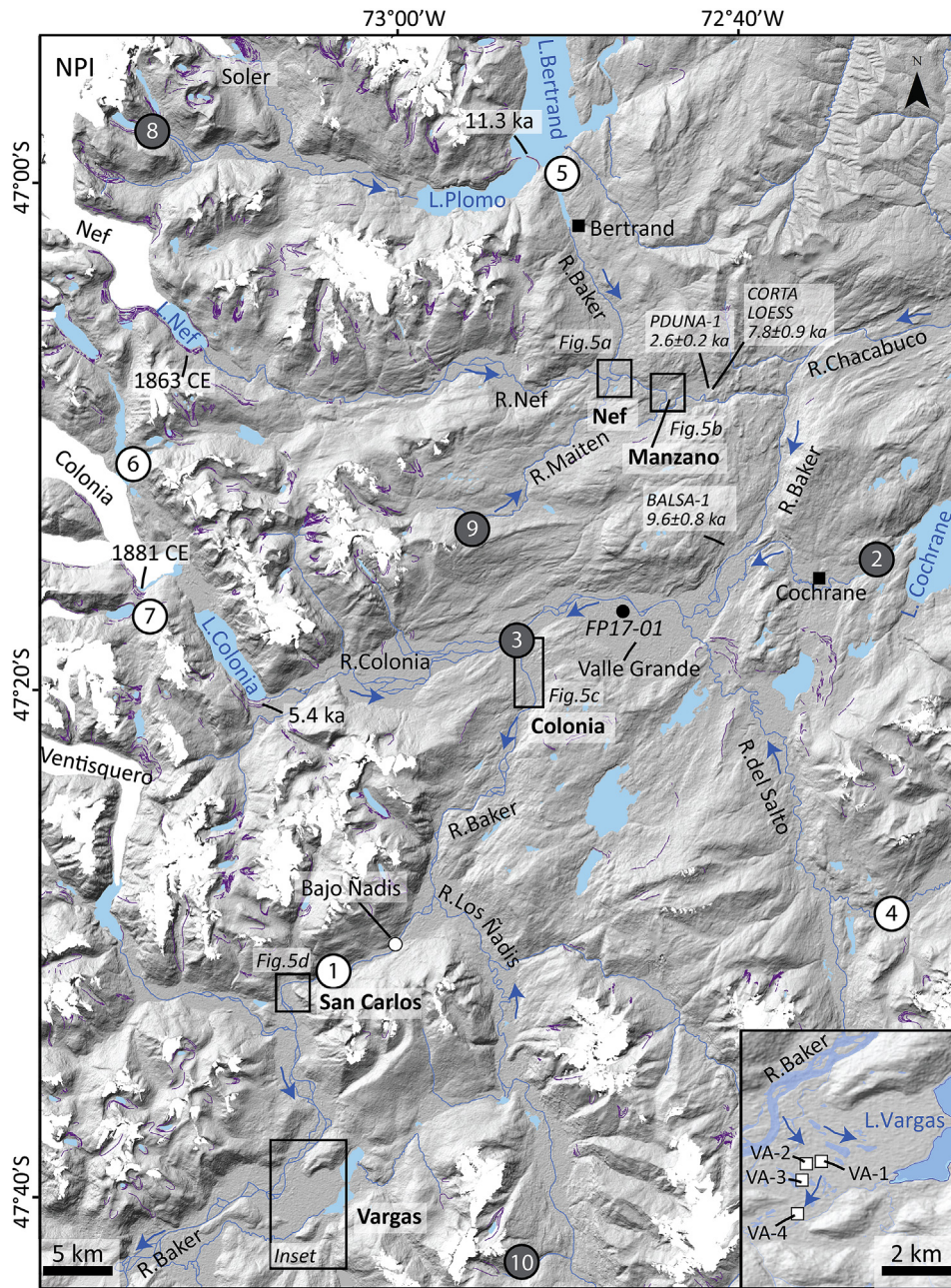


Fig. 2. Study reaches (rectangles) in the Baker valley between Lago Bertrand and Vargas. Locations of known ice dammed GLOFs are indicated with white circles, while moraine-breached GLOFs are shown by grey circles. The GLOF locality numbers relate to Table 1 where further details (including timings) on the GLOFs are presented. The Randolph Glacier Inventory glacier outlines are shown (white) as are mapped moraines (purple) from Bendle et al. (2017b). Inset: the location of the sedimentary sections analysed at the Vargas reach. Some key published ages discussed in the text are also presented, as are three OSL dates (this study) located outside the study reaches. The location of the FP17-01 core of Vandekerckhove et al., 2020 is also shown. (For interpretation of the references to colour in this figure legend, the reader is referred to the web version of this article.)

Carrera/Buenos Aires (Fig. 1) - this marking the onset of the Last Glacial Interglacial Transition (LGIT) in the region (Bendle et al., 2019). The main pattern of temperature change during the LGIT (defined as 18.0–8.0 ka) was one of a warming regional climate signal interrupted by the Antarctic Cold Reversal, which saw a glacier re-advance at ~14.0–12.8 ka (Davies et al., 2018; Sagredo et al., 2018). The region is also sensitive to shifts in the latitudinal position of the Southern Westerly Winds, a major driver of regional precipitation, which can influence Southern Hemisphere glacier mass balance (Kaplan et al., 2020).

According to the PATICE synthesis of Patagonian palaeoglacier records (Davies et al., 2020) there were four main phases of

Holocene glacier readvances or stillstands across Patagonia: 11 ka, 6–4 ka, 2–1 ka and 0.5–0.2 ka. In central Patagonia, the evidence from dated moraines formed by outlet glaciers of the Northern Patagonia Icefield and Monte San Lorenzo ice-cap (Fig. 1) broadly fit with this pattern (Glasser et al., 2012; Nimick et al., 2016; Sagredo et al., 2018). During the 21st century in Patagonia, the NPI had, in absolute values, the highest ice area reduction since the LIA (Meier et al., 2018), and the area occupied by proglacial and ice-proximal lakes increased from 112 km² in 1987 to 198 km² in 2015 (Davies et al., 2020).

With regards to regional vegetation, the valleys of the main trunk of the Río Baker and its tributaries are characterised by

temperate evergreen *Nothofagus* forest (Gut, 2008). Located within this ecotone, a pollen record from Lago Augusta in the Chacabuco valley (Fig. 1) records low arboreal cover ~16.0 cal kyr BP, with increasing evergreen forest taxa from 15.6 cal kyr BP to 13.4 cal kyr BP. *Nothofagus* increased at 11.8 cal kyr BP reaching its peak at 9.8 cal kyr BP, interpreted as the establishment of *Nothofagus* forests resulting from a warmer climate with reduced precipitation (Villa-Martínez et al., 2012). There was then little variation in *Nothofagus* abundance during the Holocene until the arrival of settlers in the early 20th century. The stability of the *Nothofagus* vegetation during the Holocene was attributed to the transitional nature of *N. pumilio*, which occurs in sectors of Central Patagonia with a precipitation range of 400–1000 mm/a (Villa-Martínez et al., 2012).

There are three main soil orders in the study region, namely entisols, inceptisols and histosols (Casanova et al., 2013). Entisols develop on fluvial sand and gravel parent material, and are characterized by a very weak profile, denoting an incipient stage of development. The characteristic entisol (*Typic Udorthent*) contains an ochric epipedon over a silty sand C horizon. These soils are saturated with water at least 20–30 days each year and occupy sites with low slope (<5–10%) on floodplains and fluvial terraces. Histosols, rich in organic matter, accumulate below the water table as peat, and typically occupy kettle hole depressions and flood basin sites (wetlands, peat bogs and swamps). In the Baker valley, histosols may reach more than 4 m in depth and started forming during the initial stages of deglaciation (Pfeiffer et al., 2010). Inceptisols (*Typic Dystrudept* and *Lithic Dystrudept*) occupy areas of bedrock hills and hummocks with a gentle slope, often related to valley-side, glacially scoured bedrock landscapes such as roches mountonées (Pfeiffer et al., 2010). Inceptisols form rapidly from coarse gravelly parent material, developing a weak B horizon with scarce clay and organic accumulation.

2.2. Modern flow regime of the Río Baker

The present-day mean annual flow of the Río Baker is 1100 m³/s making it Chile's largest river in terms of annual discharge (Dussaillant et al., 2012). As the Río Baker is mainly lake fed, the river has a regular base flow of ~500–700 m³/s (Fig. 3), with discharges reaching ~1500 m³/s during a typical spring melt season (November–December). At the Colonia reach (Fig. 2), the mean annual flood is ~1850 m³/s (Fig. 3a). The maximum flood discharges in the instrumental record (1963–2020) according to flood-type were: a) snowmelt (2684 m³/s; Feb 2009); b) rainfall (2200 m³/s; Mar 1966); c) rain on snow (2276 m³/s; Dec 1976), and d) outburst floods (>3812 m³/s, with an extrapolated hydrograph peak ~4100 m³/s; Mar 2009). In total twenty-seven outburst floods from Lago Cachet II in the Colonia valley (Site 6, Fig. 2) occurred during 2008–2017, causing peak flows of the Río Baker to reach ~2000–4000 m³/s, with sixteen of these events exceeding 2684 m³/s, the largest hydrometeorological flood on record (Fig. 3).

2.3. Glacier outburst floods of the Baker catchment

The known glacier lake floods of the Baker valley are shown in Table 1 (with locations indicated in Figs. 1 and 2), which uses the database of modern and historical floods compiled by Carrivick and Tweed (2016), augmented with events reconstructed using geomorphological evidence (Martin et al., 2019; Thorndycraft et al., 2019; Benito and Thorndycraft, 2020). In addition to the repeated flooding of Lago Cachet II (Site 6, Figs. 1 and 2), illustrated by the hydrographs in Fig. 3b, other ice-dammed lake floods in the Baker catchment include at least 39 outburst floods between 1881 and 1967 (Carrivick and Tweed, 2016) from Lago Arco in the Colonia

valley (Site 7, Fig. 2). Moraine-breaches have been documented in the Soler (Site 8, Fig. 2; Aniya and Naruse, 2001; Iribarren Anacona et al., 2015), Engaño (Site 15, Fig. 1; Iribarren Anacona et al., 2014), Leones (Site 12, Fig. 1; Harrison et al., 2006) and Los Ñadis valleys (Site 10, Fig. 2; Carrivick and Tweed, 2016).

Geomorphological evidence points to a number of outburst floods (Table 1, Fig. 2) following the end of the Antarctic Cold Reversal around 12.8 ka (Thorndycraft et al., 2019). The largest water volume released down the lower Baker valley was from the drainage of palaeolake Chelenko (Site 1, Figs. 1 and 2). This likely breached in the lower Baker, upstream of a wide, forested valley, which limits geomorphological evidence of the downstream flooding from this drainage event (Thorndycraft et al., 2019). The largest reconstructed glacier outburst flood was the Bertrand-Baker flood (Site 5, Figs. 1 and 2), with a minimum peak discharge of 110,000 m³/s. This flood was caused by drainage of ~100 km³ of lake water from Lago General Carrera/Buenos Aires (Benito and Thorndycraft, 2020), and herein we refer to new dating evidence for this event. Geomorphological evidence also exists for outburst floods from Lago Cochrane/Pueyrredón (Benito and Thorndycraft, 2020) (Site 2, Fig. 2), and palaeolake Tranquilo (Site 4, Fig. 2), dammed by the Calluqueo glacier sourced from Monte San Lorenzo (Martin et al., 2019).

To date, the longest palaeoflood record is from a palaeochannel archive in Valle Grande (Core FP17-01, Fig. 2), which records two inferred phases of increased glacier outburst flooding, at 2.57–2.17 cal kyr BP and 0.75–0 cal kyr BP (Vandekerkhove et al., 2020). However, no palaeodischarge data is presented and, given the site of deposition is flooded by modern floods from Cachet II (with floodwaters flowing upstream from the Colonia into Valle Grande), it is likely the lower elevation deposits dating to 2.57–2.17 cal kyr BP could also be inundated by rainfall and snowmelt floods based on the instrumental flood series (Fig. 3).

2.4. Study reaches

We chose five study reaches in the Baker catchment, four located on the main river, and one in the lower Nef tributary (Fig. 2). Two sites occur in the upper Baker catchment. The Nef site is located in a zone of eddy flow circulation during flooding (Benito and Thorndycraft, 2020), immediately upstream of a narrow gorge reach, and 600 m upstream of the confluence with the Baker (Fig. 2). A 15 m high sediment exposure is located in a zone of back-flooded eddy circulation on the right bank of the river. The Manzano reach is located on the Río Baker 3.5 km downstream of the Nef confluence (Fig. 2). The Angostura Chacabuco gauge station is located in the main hydraulic control section of the reach. In a zone of canyon expansion, exposures on the left margin of the river (LF1 to LF3 sites) feature three separate terraced benches (cf. Benito et al., 2003), the highest of which is ~20 m above present water level (a.w.l.).

The Colonia reach is located downstream of the Colonia-Baker confluence (Fig. 2) and features multiple river bank exposures spaced over a 4.5 km length of river, the downstream limit of which is defined by a narrow bedrock hydraulic control section. Herein we report on four stratigraphic sections from the reach. The Colonia gauge station of the Río Baker is located within this study reach.

Further downstream, the San Carlos site is located between the left bank Los Ñadis and the right bank Ventisquero tributaries (Fig. 2). Here, sediment exposures occur in a scarp slope rising up from the edge of the floodplain. This site is located in a zone of canyon expansion and the highest slackwater deposits (SWDs) were deposited on megaflood-type flood bars (Benito and Thorndycraft, 2020). The most downstream study site occurs in a zone of valley expansion near Lago Vargas (Fig. 2), where four

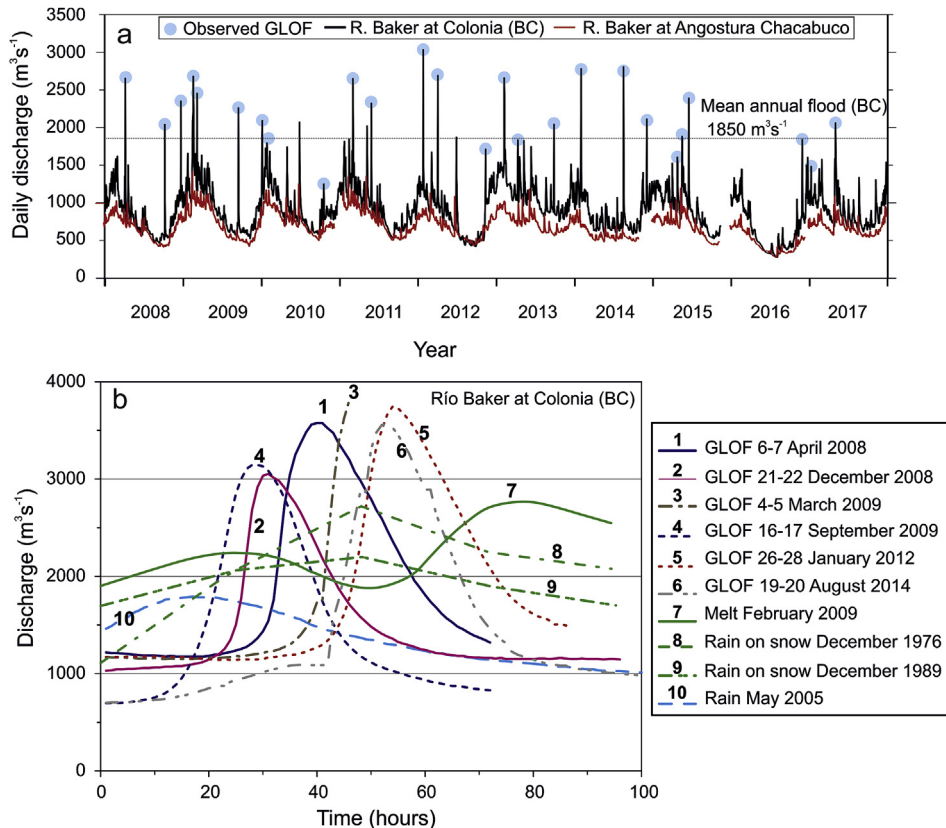


Fig. 3. a) Daily mean discharge (2008–2017) of the Río Baker downstream of the Colonia River junction (Colonia gauge station, Fig. 4c) recording GLOFs from Lago Cachet II, compared to the discharge record at El Manzano bridge (Angostura Chacabuco gauge station, Fig. 4b), which had no GLOF peaks during this period. Note that data gaps at the Río Baker Colonia (BC) station were filled using the Río Baker Bajo Nadis (Fig. 2) gauge station ($R^2 = 0.81$). b) Selection of Lago Cachet II-sourced GLOF hydrographs at the Colonia gauge station of the Río Baker compared to some typical floods produced by snowmelt, rain, or combined rain over snow events.

shallow quarries provided sections cut in flood deposits. The area features a broad alluvial surface, ~10 m a.w.l., featuring wetlands developed within catastrophic flood erosional and depositional landforms. Here, the wider valley accommodation spaces afford preservation of high magnitude Holocene GLOF sediments as the flow emerged from steeper and narrower reaches upstream (see flow directions indicated on Fig. 2 inset).

3. Methodology

3.1. Geomorphological mapping and palaeoflood stratigraphy

Fluvial landforms were mapped in ArcGIS v10.1 from aerial ortho-photographs (1:5000 in scale), supported with 1 and 5 m contour interval topographic maps, as well as ESRI™ World imagery datasets (mainly ~1m DigitalGlobe and GeoEye IKONOS imagery), and GoogleEarthPro™ imagery prior to field work. We carried out a total of five field campaigns between April 2011 and November 2017 in order to verify fluvial landforms at the five study reaches, and collect samples for geochronology. The elevations of fluvial landforms in the Baker-Colonia sector were mapped using a differential GPS (Leica). Here, the river channel bottom was surveyed using an echosound device mounted in a small boat and connected to the rover GPS, the data collected using a navigation software. At the other study reaches, hand held GPS units were used to locate mapped landforms, while bathymetric data was obtained from unpublished reports.

Field mapping and reconnaissance allowed identification of the best sections for detailed sedimentological and stratigraphic

descriptions to compile palaeoflood stratigraphies. The sedimentological evidence of past floods included slackwater flood deposits and overbank floodplain sediments, both used as palaeostage indicators of past floodwater elevations (Kochel and Baker, 1982; Benito and Thorndycraft, 2005; Baker, 2008). Detailed stratigraphic analyses were carried out at 15 stratigraphic profiles across the five study reaches. Individual flood-beds were distinguished through a variety of sedimentological indicators including: clay layers at the top of a flood-bed, buried palaeosols, bioturbation indicating the exposure of a sedimentary surface, stone layers, and changes in sediment colour (Baker and Kochel, 1988; Thorndycraft et al., 2004). Palaeosol samples were collected for geochemical analysis. Palaeosol diagnostic horizons, where possible, were classified using a simplified key to Soil Taxonomy orders (Soil Survey Staff, 2014) suggested by Retallack (2001).

3.2. Geochronology

Palaeoflood chronology was determined using radiocarbon and OSL dating of samples collected from individual flood-beds or palaeosols. In total 23 radiocarbon AMS analyses were carried out (Table 2) at two laboratories: (1) the Spanish Accelerator Centre in Seville (CNA), and (2) the Poznan Radiocarbon Laboratory (Poz). Radiocarbon dates are quoted in the text as the two-sigma calibrated age range (95%). Radiocarbon ages were calibrated to calendar ages using Oxcal 4.4 software (Ramsey, 2001) based on Hogg et al. (2020) calibration data set SHCal20 (Table 2).

OSL analyses were carried out at the Radioisotopes Unit of the University of Seville. OSL dating was completed for a total of 14

Table 1

Summary of modern and palaeo-GLOFs recorded or reconstructed from geomorphological evidence in the Río Baker catchment. Site numbers refer to the labels on the maps in Figs. 1 and 2.*Dam type inferred from geomorphological evidence but actual type or locality not confirmed e.g. due to lack of field access.

Site	River (lake)	Type of dam	Evidence	Timing	References
1	Baker (Palaeolake Chelenko)	Ice*	Palaeoshorelines & raised deltas	12.4–11.8 ka	Thorndycraft et al. (2019)
2	Cochrane (Lago Cochrane/Pueyrredón)	Moraine	Boulder bars at downstream of contemporary lake outlet.	11.8–9.6 ± 0.8 ka	Thorndycraft et al. (2019)
3	Baker (Palaeolake Colonia/Valle Grande)	Moraine	Raised delta. Boulder bars downstream of incised moraine	11.8–9.6 ± 0.8 ka	Thorndycraft et al. (2019)
4	del Salto (Palaeolake Tranquilo)	Ice	Palaeoshorelines, deltas, incised bedrock	~12.0 ka	Martin et al. (2019)
5	Baker (Lago General Carrera/Buenos Aires)	Ice* (authors mapped an eroded moraine upstream from likely ice dam location)	Boulder bars, incised bedrock, eddy deposits	9.6 ± 0.8 ka	Benito and Thorndycraft (2020) This paper
6	Colonia (Lago Cachet II)	Ice	Observed GLOFs	2008–2017	Dussaillant et al. (2009); Jacquet et al. (2017)
7	Colonia (Lago Arco)	Ice	Observed GLOFs	1881–1967	Tanaka (1980); Carrivick and Tweed (2016)
8	Soler (Laguna del Cerro Largo)	Moraine	Observed GLOF	March 16, 1989	Aniya and Naruse (2001), Iribarren Anacona et al. (2014)
9	Maiten	Moraine	Unknown to authors	Between 2000 and 2003	Carrivick and Tweed (2016)
10	Los Ñadis	Moraine	Unknown to authors	Between 1987 and 1998	Carrivick and Tweed (2016)
11	Viviano	Moraine	Unknown to authors	Between 1987 and 1998	Carrivick and Tweed (2016)
12	Leones (Lago Calafate)	Moraine	Observed GLOF	June 22, 1905	Carrivick and Tweed (2016)
13	Aviles (Laguna Bonita)	Moraine	Unknown to authors	Between 2002 and 2008	Carrivick and Tweed (2016)
14	Pedregoso	Moraine	Unknown to authors	Between 1985 and 1987	Carrivick and Tweed (2016)
15	Engaño	Moraine	Observed GLOF	July 16, 1955 & March 11, 1977	Iribarren Anacona et al. (2014); Carrivick and Tweed (2016)

sand samples (Table 3) collected in the field using PVC cylinders to avoid exposure of the sediment to white light. Quartz grain fractions of size 180–250 μm were extracted from each sample for luminescence measurements. Equivalent doses, i.e. the doses accumulated over the burial time, were measured on 40 to 70 small multi-grain aliquots of each sample. These aliquots, containing <20 grains each, allow sufficient resolution to detect extrinsic effects like incomplete bleaching (Medialdea et al., 2014). Luminescence measurements were carried out in an automated Risø OSL/TL reader (TL-DA 20) with a calibrated $^{90}\text{Sr}/^{90}\text{Y}$ beta source. Dose recovery tests have been used to determine the most appropriate measurement conditions and confirm the suitability of the method to accurately recover a given dose. Equivalent doses were estimated using the Central Age Model (Galbraith et al., 1999) on the dose distributions. Data was reduced to limit the scatter in the dose distributions by removing outliers following 1.5 times the Inter Quartile Range established for boxplots (Tukey, 1977). Estimated equivalent doses for the 14 samples are summarized in Table 3.

Beta and gamma dose rates were based on the radionuclide activity concentration derived from high resolution gamma spectrometry measured on ~100 g of bulk material from the sediment matrix of each sample (Table 3). The contribution of cosmic radiation has been calculated according to a varying burial depth beneath ground surface (Prescott and Hutton, 1994). Sampling depth and total dose rates for an infinite matrix, and the derived age estimates are summarized in Table 3.

3.3. Palaeodischarge quantification

Palaeoflood discharge estimates were based on the assumptions that: a) the elevation of a flood-bed relates to a minimum flood stage reached by a past flood event; or b) a palaeosol provides a non-exceedance, upper bound, flood stage (Baker, 1987). Our

modelling approach assumes (cf. O'Connor and Webb, 1988) that: (1) the peak discharge was of sufficient duration to have simultaneously affected the entire modelled reach; (2) streamlines are parallel and cross-sections were defined at sufficiently short intervals to maintain flow hydraulic characteristics; and (3) there are minimum topographic changes (non-deformable boundaries) at the study reaches. Modern ice-dammed lake flood hydrographs from Lago Cachet 2 showed sustained peak flow discharges for at least 4–5 h which fulfil the steady flow assumption (1) at reach scale. Flow separation zones, where parallel streamlines are an inappropriate assumption (2) such as at the sites of flood sediment deposition, were denoted as ineffective flow areas in the model, so do not contribute to convey flow. To limit the effect of topographic changes (assumption 3) we have selected sites associated with narrow bedrock control sections, and where there was good geomorphological evidence constraining bedrock incision caused by the Bertrand-Baker catastrophic flood (Benito and Thorndycraft, 2020). The palaeoflood stage of each flood-bed (upper contact) in the stratigraphy was converted into a discharge value through hydraulic modelling. We used one dimensional hydraulic flood modelling using GeoHEC-RAS software (O'Connor and Webb, 1988; Hydrologic Engineering Center, 2010). This model generates water surface profiles for given discharges associated with gradually varied flows, using the hydraulic step-backwater calculation (Chow, 1959). The computed water surface profile matching the elevation of the upper flood-bed contact yields an estimation of the minimum palaeoflood discharge, as the water surface is an unknown depth above the sediments. While 2D modelling has been used to study the complex hydraulics of modern GLOFs (e.g. Carrivick, 2006), such modelling requires flood hydrograph data not available for palaeofloods, so given those limitations, 1D modelling is an effective tool for quantifying robust palaeodischarge estimates.

Four hydraulic models were developed: 1) Nef reach (Fig. 4a); 2)

Table 2

Radiocarbon dating, with indication of the stratigraphic profile names and unit number. Radiocarbon ages were calibrated to calendar ages using OXCAL software (Ramsey, 2001) using the Hogg et al. (2020) calibration data set SHCal20. Some conventional ^{14}C BP dates have multiple intercepts in the calendar year BP curve. Two Sigma calibrated age is provided in ranges with indication of their relative area (in %) under 2σ distribution. The modern radiocarbon dating (Raices profile sample RA-13) was calibrated using Bomb13H12, and the age in years BP was given in negative numbers (post 1950).¹ The laboratory code refers to the following radiocarbon dating facilities: CNA: Spanish Accelerator Centre in Seville; Poz: Poznan Radiocarbon Laboratory.

Flood-bed	Latitude	Longitude	Sample material	Lab code ¹	Age, ^{14}C yr BP	$\delta^{13}\text{C}$ ‰	Calibrated age (2σ) BP (95.4%)	Calibrated age (2σ) CE (95.4%)	Reported age (2σ) cal BP (95.4%)
Nef reach									
NE-99	-47.12599	-72.77957	Charcoal	CNA-4601	860 \pm 30	-25.63	790-780 (1.4%) 770-670 (94.0%)	1160-1280 CE	670-790
Baker-Manzano reach									
ST1-02	-47.13613	-72.73584	Charcoal	CNA-4600	2560 \pm 30	-26.51	2750-2485 (94.4%) 2480-2465 (1.1%)	805-560 BCE	2465-2750
LF1-27	-47.13131	-72.72956	Charcoal	CNA-2790	2544 \pm 34	-23.09	2740-2425	795-475 BCE	2425-2740
LF2-04	-47.13151	-72.72941	Charcoal	CNA-4373	950 \pm 30	-24.92	910-735	1040-1215 CE	735-910
LF3-02	-47.13162	-72.72952	Charcoal	CNA-2795	2115 \pm 31	-27.07	2125-1990 (88.6%) 1965-1930 (6.9%)	175 BCE-20 CE	1930-2125
LF3-08	-47.13162	-72.72952	Charcoal	CNA-2794	1672 \pm 32	-26.17	1590-1420	360-530 CE	1420-1590
LF3-10	-47.13162	-72.72952	Charcoal	CNA-3316	1485 \pm 32	-27.17	1405-1390 (3.0%) 1380-1290 (92.4%)	545-660 CE	1290-1405
LF3-12	-47.13162	-72.72952	Charcoal	CNA-2793	1242 \pm 32	-25.35	1260-1245 (1.6%) 1230-1210 (1.7%) 1180-1050 (86.5%) 1020-985 (5.7%)	690-965 CE	985-1260
LF3-18	-47.13162	-72.72952	Charcoal	CNA-2791	634 \pm 30	-26.96	650-585 (63.4%) 575-535 (32.1%)	1300-1415 CE	535-650
LF3-27	-47.13162	-72.72952	Charcoal	CNA-2792	692 \pm 31	-25.15	665-555	1285-1395 CE	555-665
Baker-Colonia reach									
LV-PS1	-47.33135	-72.850788	Charcoal	Poz-42329	6160 \pm 40	-25.3	7165-6940	5220-4990 BCE	6940-7165
LV-03	-47.33135	-72.850788	Charcoal	Poz-42326	5295 \pm 35	-19.8	6195-5990 (91.1%) 5965-5940 (4.3%)	4245-3995 BCE	5940-6195
LV-04	-47.33135	-72.850788	Charcoal	Poz-42327	4735 \pm 35	-25.9	5585-5440 (65.6%) 5405-5325 (29.9%)	3635-3375 BCE	5325-5585
LV-12	-47.33135	-72.850788	Charcoal	Poz-42328	570 \pm 30	-27.8	645-585 (57.7%) 570-525 (37.7%)	1305-1425 CE	525-645
LV-13	-47.33135	-72.850788	Charcoal	Poz-44767	200 \pm 30	-27.3	310-255 (26.3%) 225-135 (54.8%) 35- (14.4%)	1640-1815 CE (81.1%)	135-310 (81.1%)
LB-10/PS2	-47.32504	-72.85844	Charcoal	Poz-42320	2545 \pm 35	-25.4	2755-2680 (39.1%) 2645-2610 (14.8%) 2600-2490 (41.6%)	805-545 BCE	2490-2755
LB-11	-47.32504	-72.85844	Charcoal	Poz-42321	610 \pm 30	-27.2	655-545	1295-1405 CE	545-655
LB-12	-47.32504	-72.85844	Charcoal	Poz-44765	240 \pm 40	-33.9	435-360 (15.0%) 330-260 (40.1%) 225-140 (34.4%) 30- (5.9%)	1515-1810 CE (89.5%)	140-435
LB-13	-47.32504	-72.85844	Charcoal	Poz-44766	105 \pm 30	-28.9	270-210 (25.9%) 150-10 (69.5%)	1680-1940 CE	10-270
RA-02	-47.30852	-72.86674	Charcoal	Poz-42324	2490 \pm 30	-25	2725-2460 (94.2%) 2450-2430 (1.3%)	775-485 BCE	2430-2725
RA-07	-47.30852	-72.86674	Charcoal	Poz-42325	470 \pm 30	-23.3	545-490	1405-1460 CE	490-545
RA-12	-47.30852	-72.86674	Charcoal	Poz-42339	140 \pm 30	-29	280-170 (37.2%) 155-5 (58.3%)	1670-1945 CE	5-280
RA-13	-47.30852	-72.86674	Charcoal	Poz-42340	104.47 \pm 0.34 pMC	-22.1	(-6)- (-7) (67.4%) (-60)- ... (28%)	1957 CE	-7

Manzano reach (Fig. 4b); 3) Colonia reach (Fig. 4c), and 4) San Carlos-Vargas reach (Fig. 4d). For each modelled reach a 10 m DTM was created in ArcMap 10.1 from 5 m contours from which cross-sections were extracted using HEC-GeoRAS tools (Hydrologic Engineering Center, 2011, Fig. 4). Subcritical flow conditions were assumed along the surveyed study reaches, with normal flow selected as the boundary condition in all reaches except at Manzano where the Río Baker Angostura Chacabuco gauge station rating curve was used, as it is located at the downstream end of the

reach (Fig. 4b). The assigned Manning's n values were 0.03–0.035 for bedrock channels, 0.025–0.03 for sandy channels, 0.045–0.05 for sandy and bedrock talus slopes with sparse vegetation, and 0.05–0.06 for sandy bars and channel margins with dense vegetation. Model calibration was performed at the Baker-Colonia reach using the Colonia gauge station rating curve (Fig. 4c). At the other sites, field survey of water surface elevation was used to tune up the reach model. A sensitivity test performed on the model shows that for a 25% variation in the roughness n values, only a 1–5% change is

Table 3

Summary of total dose rates, estimated equivalent doses based on OSL measurements and derived ages.

Sample	Longitude	Latitude	Depth (m)	Dose rate (Gy/ka)	Equivalent dose (Gy)	Age (ka)
Nef reach						
NE-07	-47.12599	-72.77957	11.5	3.26 ± 0.12	8.0 ± 0.4	2.4 ± 0.1
Baker-Manzano reach						
ST1-01	-47.13613	-72.73584	0.6	2.47 ± 0.11	16.8 ± 0.8	6.8 ± 0.4
ST1-02	-47.13613	-72.73584	0.3	3.47 ± 0.13	13.4 ± 0.5	3.9 ± 0.2
ST5-01	-47.13590	-72.73167	0.4	2.47 ± 0.09	15.7 ± 0.9	6.4 ± 0.4
LF1-01	-47.13131	-72.72956	1.2	5.00 ± 0.23	21.7 ± 1.2	4.3 ± 0.3
LF1-26	-47.13131	-72.72956	1.1	4.16 ± 0.18	18.2 ± 1.7	4.4 ± 0.4
LF1-28	-47.13131	-72.72956	0.8	4.91 ± 0.25	10.0 ± 4.4	2.0 ± 0.9
LF2-01	-47.13151	-72.72941	2.9	4.78 ± 0.21	10.6 ± 0.5	2.2 ± 0.1
LF2-14	-47.13151	-72.72941	0.9	4.16 ± 0.18	30.3 ± 1.0	7.3 ± 0.4
San Carlos-Vargas reach						
SC-04	-47.52586	-73.04965	0.9	2.73 ± 0.13	14.1 ± 0.2	5.2 ± 0.3
SC-05	-47.52586	-73.04965	0.7	2.95 ± 0.14	16.3 ± 0.4	5.5 ± 0.3
Catastrophic flood sediments						
Balsa-1	-47.22878	-72.65428	3.0	2.11 ± 0.10	20.3 ± 1.3	9.6 ± 0.8
Aeolian deposits						
Corta-Loess	-47.13001	-72.68843	0.7	2.67 ± 0.12	20.8 ± 0.9	7.8 ± 0.9
PDuna-1	-47.13030	-72.69295	1.3	4.76 ± 0.18	12.2 ± 1.0	2.6 ± 0.2

introduced into the calculated discharge results. Rating curves relating individual stratigraphic flood-bed elevations to HEC-RAS model outputs were generated at each site. Minimum flood discharges associated with the elevation of the upper contact of each sedimentary unit were estimated in addition to the flood magnitudes associated with non-exceedance bounds. Flood water surface elevation and depth flow raster maps were created in Ras Mapper and ArcGIS for selected flood discharges.

4. Results

In this section we firstly outline the main geomorphology we mapped in the Baker valley, and report on geochronology from landforms not located in the main palaeoflood study reaches (Section 4.1). The geomorphology of the study reaches is informed by our classification of fluvial landforms in to megaflood-type, resulting from catastrophic floods, and Holocene alluvial sediments, including slackwater deposits (SWDs) from extreme floods (Benito and Thorndycraft, 2020). Section 4.2 describes the main diagnostic palaeosols identified in the field, and weathering indicators developed within flood-beds that evidence time lag between events and correlation among stratigraphic profiles. In Section 4.3 we describe the flood stratigraphy and geochronology at key stratigraphic sections at the five study reaches before turning to flood magnitude and palaeodischarge quantification through hydraulic modelling (Section 4.4).

4.1. Geomorphological mapping

The geomorphological maps of the four study reaches are presented in Fig. 5. The fluvial landforms were divided in to three main types (cf. Benito and Thorndycraft, 2020): (i) inner gorge bedrock erosion; (ii) gravel and sand bars, at elevations of up to 70 m a.w.l., usually located in wider valleys upstream (e.g. Fig. 6c, g and 6h) or downstream (e.g. Fig. 5b) of gorge reaches; and (iii) silt and fine sand fluvial sediments deposited up to 35 m a.w.l. in slackwater environments (e.g. Fig. 6a, b, 6d-6f, 7a-7e). Landforms (i) and (ii) were interpreted as megaflood-type landforms, resulting from catastrophic flooding, while (iii) comprise Holocene alluvial landforms from low to extreme flood magnitudes (Benito and Thorndycraft, 2020).

The four geomorphological maps presented in Fig. 5 demonstrate flood-incised bedrock forming vertically walled channel

incision (up to 25 m deep), known as inner channels, produced by recession of headward erosion (Benito and Thorndycraft, 2020) along the narrowest sections of the Baker and Nef rivers. In the case of the Nef, Manzano and Colonia reaches (Fig. 5a–c) these narrow reaches provide downstream control sections that allow backflooding during flood events, and the deposition of fine grained flood sediments that we utilise to develop our palaeoflood stratigraphy (Section 4.2).

At the Manzano reach (Fig. 5b) we mapped longitudinal, pendant and eddy bars. The lowest elevation eddy bars sit on top of the eroded inner channels of the Baker, and beneath the three flood benches at the La Fortuna site (LF1-LF3, Figs. 5 and 6) that we describe in Section 4.2. Longitudinal bars, of megaflood-type landforms, are usually located at channel margins and are generally associated with steep bedrock reaches. At the Manzano reach at the point the Baker emerges from a gorge (Fig. 5b), elongated gravel bars up to 30 m a.w.l. are capped with imbricated boulders. Pendant bars were formed downstream of bedrock obstacles (Baker, 1973), such as valley floor roche moutonées (Fig. 5b). Pendant bars typically consisted of coarse and poorly sorted gravels and boulders with downstream directed foresets.

Eddy bars typically occur on the valley margins and along the lower courses of back-flooded tributaries, such as the Nef and Maiten (Fig. 5a). We used OSL to date an eddy bar located on the western valley margin (Fig. 2, West of Cochrane), ~0.5 km downstream from an expansion bar with imbricated boulders likely formed from a reworked moraine (Thorndycraft et al., 2019). A 7 m high quarry exposure reveals, in the upper 4 m, four facies composed of fine gravel and coarse sand with foresets dipping upstream, indicating a reverse current and eddy circulation (Fig. 6h). The dated sample was taken 3 m below the surface and gave an age of 9.6 ± 0.8 ka (Figs. 2 and 6h; Table 3 Balsa-1). We also constrained the age of an eddy bar by OSL dating of loess sediment draped on top of the bar, downstream of the Manzano reach (Corta-Loess, Fig. 2; Table 3). This sample was dated to 7.8 ± 0.9 ka, providing a *terminus ante quem* age for eddy bar deposition (Thorndycraft et al., 2019).

Landforms of type (iii), located up to 35 m a.w.l. were interpreted as high-stage flood deposits, and they typically occur in areas of valley expansion, upstream of narrow inner-channel reaches (Fig. 5). These fine grained alluvial sediments were sometimes found deposited inset within accommodation space created by erosion of megaflood-type depositional landforms. For example,

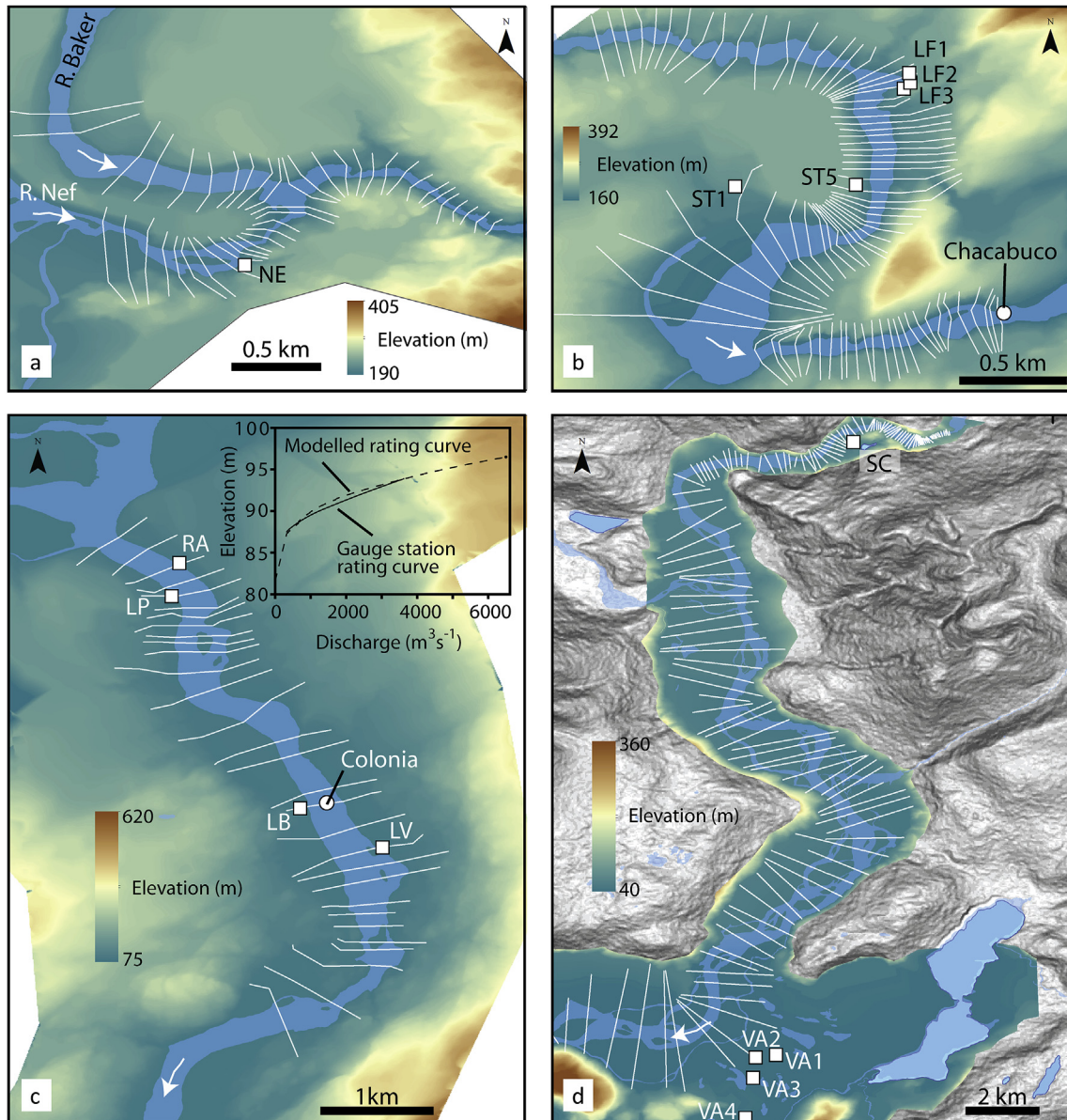


Fig. 4. The four model domains used to quantify palaeodischarges: a) Nef reach; b) Manzano reach; c) Colonia reach; d) San Carlos-Vargas reach. Note the location of the Angostura Chacabuco and Colonia gauge stations in the Manzano and Colonia reaches respectively. Each map shows the location of the sedimentary sections described in the text, and valley cross-sections used in the HEC-RAS one-dimensional flood model. The cross sections are presented on the 10 m grid DTM created in ArcGIS using 5-m contour interval topography. In the smaller scale map d), wider relief is shown using a slope DTM where lighter colours indicate flatter slopes, and darker colours steeper slopes. (For interpretation of the references to colour in this figure legend, the reader is referred to the web version of this article.)

the three Fortuna sections are inset within a scarp slope cut in catastrophic eddy bar gravels (Figs. 5b and 6d). At other sites, type-iii facies may sit on top of megaflow-type bar surfaces, for example the ST sites of the Manzano reach (Figs. 5b and 6c).

The fine grained sediments of landform type (iii) include eddy and slackwater deposits (Fig. 6), with sediments from multiple flood events preserved at sites of deposition. Individual flood-beds typically grade upwards from parallel laminated coarse-to-medium sands to ripple laminated fine sand and silt, with upper thin laminae of silt and clay (Fig. 6b). Climbing ripples in-phase or in-drift, depending on local flow velocity, indicate high suspended sediment load in the floodwater. In stacked flood layers up to 15 m thick, such as in the lower Nef (Fig. 6a), the highest elevation beds are usually thinner and the ripple part of the sequence is limited or non-existent (Fig. 6b). The lower contact of overlying beds is

usually sharp and conformable. Some flood-beds may contain fluid escape structures.

Aeolian landforms (dunes and loess) are another feature of the valley floor geomorphology, for example Benito and Thorndycraft (2020) reported valley floor dunes at Bajo Ñadis (Fig. 2). At Colonia (Fig. 5c), dunes up to 10 m in height are located at elevations below the flood-incised moraine and megaflow-type bars, and above the highest type (iii) alluvial sediments. Benito and Thorndycraft (2020) interpreted the sediment source for these dunes to derive from fine-grained sediments deposited by the Bertrand-Baker catastrophic flood. However, aeolian reworking of later Holocene flood sediments may also have occurred. For example, we obtained an OSL age of 2.6 ± 0.2 ka for a small dune downstream of the Manzano reach (PDuna-1, Fig. 2).

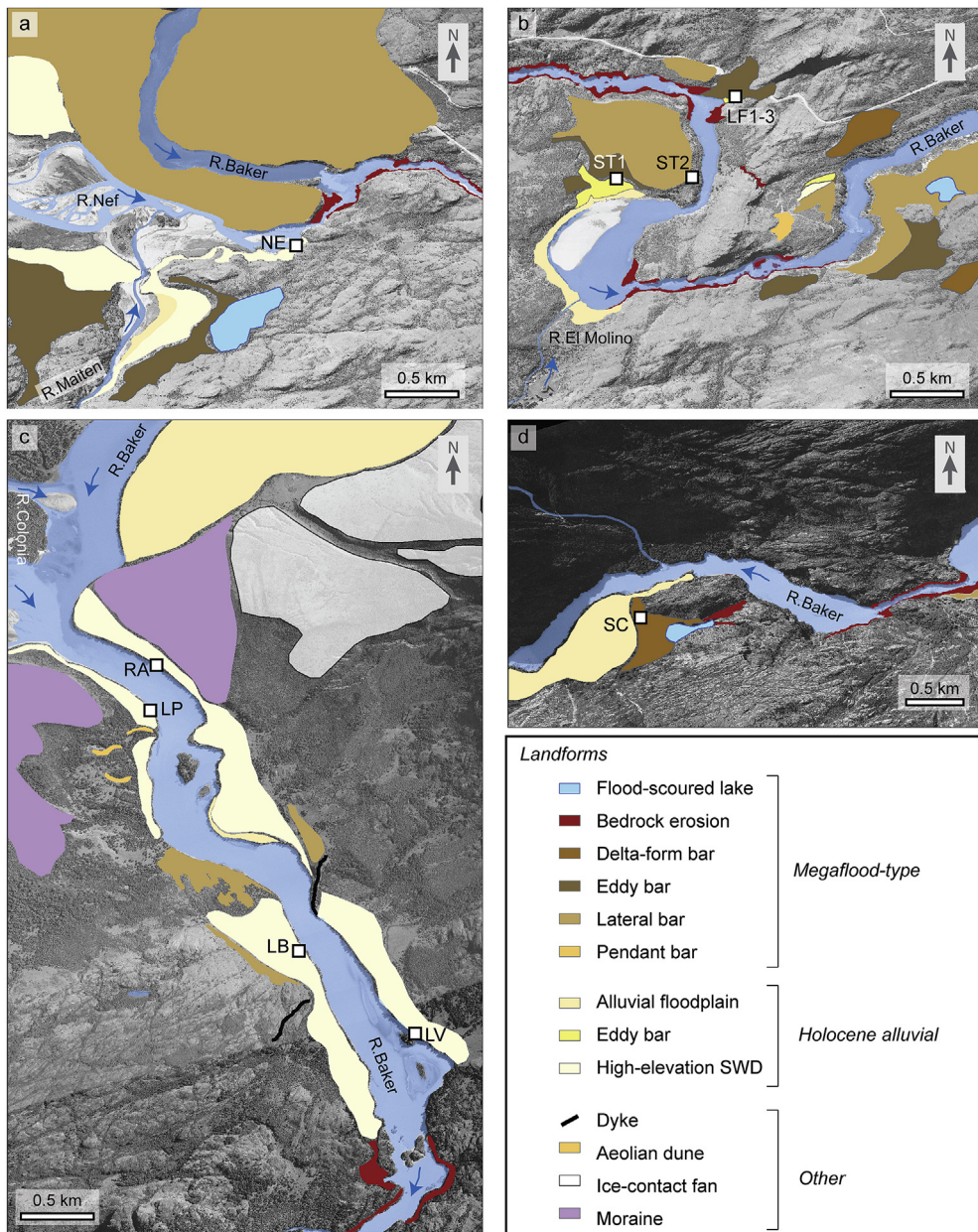


Fig. 5. Geomorphological maps of the study sites showing fluvial landforms classified as either megaflood-type or Holocene alluvial landforms at four reaches: a) the Baker-Nef confluence sector; b) the Baker-Manzano sector (downstream of a); c) the Baker-Colonia sector; and d) the San Carlos sector. Locations of the stratigraphic profiles presented in Figs. 8 and 9 are labelled.

4.2. Palaeosols

Palaeosols (Bw horizon) and other pedogenetic indicators were developed on sandy-loam flood-beds (Figs. 6 and 7). These buried soils are cumulative soil profiles developed during periods of low rates of alluviation allowing simultaneous soil formation and sediment deposition (Nikiforoff, 1949). We interpret the alluvial pedogenesis as associated to phases of low flood frequency, indicating changes in flood behaviour over time. Here, we describe some key palaeosol features, in particular based on descriptions and geochemistry from the LV profile (Colonia reach), because they were effective stratigraphic markers when determining flood stratigraphy (Section 4.3). The strongly developed PS1 and PS2 palaeosols (Fig. 7b) comprised a B-horizon (~40 cm thick), with a

dark reddish brown colour (7.5 YR to 5 YR hue), crumb to sub-angular blocky structure, and high porosity (>75%). The organic matter content is relatively high (~2.3%) as well as the concentration of Fe and Al (Table 4). The deeper C-horizon contains abundant redoximorphic features, with concretions of Fe and Mn and grey colours. The two main phases of well-developed buried soils were radiocarbon dated to 6940–7165 cal BP (PS1) and 2490–2775 cal BP (PS2) (Table 2).

Incipient soils (C-horizon) are developed within the upper 10–25 cm of some flood beds, with 5Y hue (yellowish) and coarse to very coarse crumbly structure. These incipient soils contain lower organic matter (~0.6%), maintaining features of parent material, namely relatively high concentrations of Ca, Mg, and K, and medium levels of Fe and Al (Table 4).

Table 4

Soil horizon sequence in La Valla (LV) profile (upper) and geochemical elements (below). Bw, subsurface soil horizon characterized by reddening, higher development and accumulation of clay and organic matter; C, subsurface soil horizon that may appear similar to parent material and that includes unaltered material and material in various stages of weathering. Soil location refers to stratigraphic units in Fig. 9.

Unit	Age in cal BP	Field aspect	Colour (wet)	Colour (dry)	M.O. %	C.E. (µS/cm)	pH	Horizon	Structure	Porosity
PS2	2490–2755*	Reddish	7.5YR5/8	10YR6/5	2.32	258	5.5	Bw	Coarse to medium angular blocky	>75%; coarse, charcoal
LV-3	5940–6195	Gley	5Y5/6	2.5Y6/4	0.56	218	5.6	C	Very coarse crumbly to subangular blocky	60–70%; fine-medium
LV-2	>6195 to <6940	Gley	5Y3/4	2.5Y5/4	0.59	233	5.7	C	Coarse to very coarse crumbly	50–60%; fine
PS1	6940–7165	Reddish	5YR3/4	10YR5/6	1.13	180	5.7	Bw	Coarse to medium angular blocky	>85%, coarse

Unit	Soil cations, mg/kg				Trace elements, mg/kg				
	K	Na	Mg	Ca	Mn	Fe	Zn	Cu	Al
PS2	659	100	709	365	32867	110	9.4	3.6	7902
LV-3	775	82	987	437	28250	66	6.1	2.7	4654
LV-2	523	39	594	262	23160	36	4.3	2.1	3415
PS1	346	50	197	303	23456	21	2.7	1.1	4269

4.3. Flood stratigraphy

4.3.1. Lower Nef

At the Lower Nef site (Fig. 5a) two main depositional landforms from the catastrophic Bertrand-Baker flood were formed (Site 5, Fig. 2). The first, a longitudinal bar deposit extends for ~2.5 km across the valley floor, upstream of a narrow gorge carved by inner channel erosion. The second, in the lower Maiten valley, an eddy bar ~70 m a.w.l. contains coarse sand and fine gravel with cross-bedding. Inset within these megaflood-type landforms, we mapped a set of SWD benches, the highest located ~15 m a.w.l. An exposure of this SWD bench (NE site), located 600 m upstream of the Baker-Nef confluence, was described and sampled.

The section comprises three flood benches with multiple sand layers each well marked by horizontal to undulating, though conformable, contacts (Figs. 6a and 8a). The higher bench records a minimum of 116 flood-beds. An OSL sample, 1.6 m from the base of the sequence (NE-07), was dated to 2.4 ± 0.1 ka. The flood-beds consist of medium sand with climbing ripples, indicating an upstream flow direction, grading to fine sand with parallel lamination, and silty sand to clay laminae at the top. The upper sequence contains fluid escape deformations. The flood-beds vary in thickness from 40 cm in the lower sets to 6–7 cm at the top of the outcrop. In the upper section, the repeated flood-bedding is broken by a buried light brown soil (Fig. 6b). Above this palaeosol, we identified 20 flood-beds (Fig. 8a). In flood-bed (NE-99), 0.3 m above the palaeosol, there is evidence for edaphic features with a weakly developed ochric epipedon. This layer was radiocarbon dated to 670–790 cal BP (Fig. 8a). A minimum of 18 flood-beds post-date this incipient soil.

The other two benches are inset beneath the higher bench (Figs. 6a and 8a). The middle bench records a minimum of 25 flood-beds that pinch out to the upper bench, and the lower inset bench consists of at least 15 flood units that descend in topography to an elevation of ca. 4 m a.w.l. We interpret that the lower two sand benches record a later lower magnitude glacier flood regime, a common feature of modern hydrology in the region (Dussaillant et al., 2009, 2012; Wilson et al., 2019).

4.3.2. Baker–Manzano reach

The Manzano reach comprises two narrow gorge sections, separating wider sediment accommodation zones (Fig. 5b). This physiography controls landform formation, in particular the megaflood-type landforms with inner-channel bedrock erosion occurring in the steeper gorge reaches, and longitudinal, pendant and eddy bar formation occurring downstream of narrow sections (Fig. 5b). Landform type (iii) is inset within the catastrophic flood landforms; floodplain deposits are preserved on the valley margin,

while slackwater flood deposits occur up to ~25 m a.w.l. usually draped on megaflood-type deposits. We describe the flood stratigraphy at two sites: 1) La Fortuna on the left bank, where three flood benches (LF1, LF2, LF3) overlie a gravel eddy bar; and 2) at a right bank valley embayment with four sand benches (10 m, 17.5 m, 22 m and 25 m a.w.l.) and two higher elevation deposits (ST1 and ST5) that were deposited unconformably on top of a megaflood-type gravel eddy bar deposit (Fig. 6c).

At the La Fortuna site (LF), the upper bench comprises 33 flood units divided in two sets by a buried soil (Fig. 8b, 6e). The first set contains 26 stacked sand layers, 4–10 cm in thickness, grey-whitish in colour, with some beds exhibiting ripples or wavy lamination. Contacts are clearly marked by 1–2 cm thick silt laminae with bioturbation features. Flood-beds LF1-01 and LF1-26 were OSL dated to 4.3 ± 0.3 ka and 4.4 ± 0.4 ka, respectively (Table 3). The second set contains at least seven flood-beds, of grey-whitish colour, separated by bioturbated brown sandy silt. A radiocarbon date from the PS2 palaeosol beneath this flood-bed provides a minimum age of 2425–2740 cal BP, which is further supported by an OSL date of 2.0 ± 0.9 ka from the overlying flood-bed (LF-28). The stratigraphy and geochronology, therefore, indicates a hiatus in flood deposition of likely over two millennia at this section.

The middle bench contains 21 flood events in two sets separated by an unconformity, marked by an incipient reddish soil. The flood units are 10–40 cm in thickness composed of greyish sand with well-developed climbing ripples showing reverse paleocurrent direction typical of eddy environments. The beds are separated by undifferentiated silt and very fine sand (light brown in colour), likely related to an aeolian source overprinted with edaphic alteration. In the lower section, flood-bed LF2-01 was OSL dated to 2.2 ± 0.1 ka, which correlates with flood-bed LF1-28. A radiocarbon age of 735–910 cal BP from LF2-04 (which features an incipient palaeosol) marks an increase in flood frequency at the site. We sampled LF2-14 for OSL dating, however, the age of 7.3 ± 0.4 ka is considered an outlier as it does not fit the stratigraphy and geochronology at the La Fortuna site.

The lower bench (LF3) contains 30 flood-beds each with well-marked sub-horizontal contacts, with up to six buried soils preserved (mostly ochric and melanic epipedons). The flood-beds are 10–25 cm thick and formed of fine to very fine sand with ripples and wavy structures. The first three sets show six floods over ~2125–1420 cal BP (one per 117 years), two floods over ~1590–1290 cal BP (one per 150 years), and two floods over ~1405–985 cal BP (one per 210 years). The fourth set contains six floods over the period ~1260–535 cal BP that increased the frequency to one flood per 120 years. The final set comprises nine floods in a short period, likely in less than 100 years (~650–555 cal BP), with an average of one flood per decade.

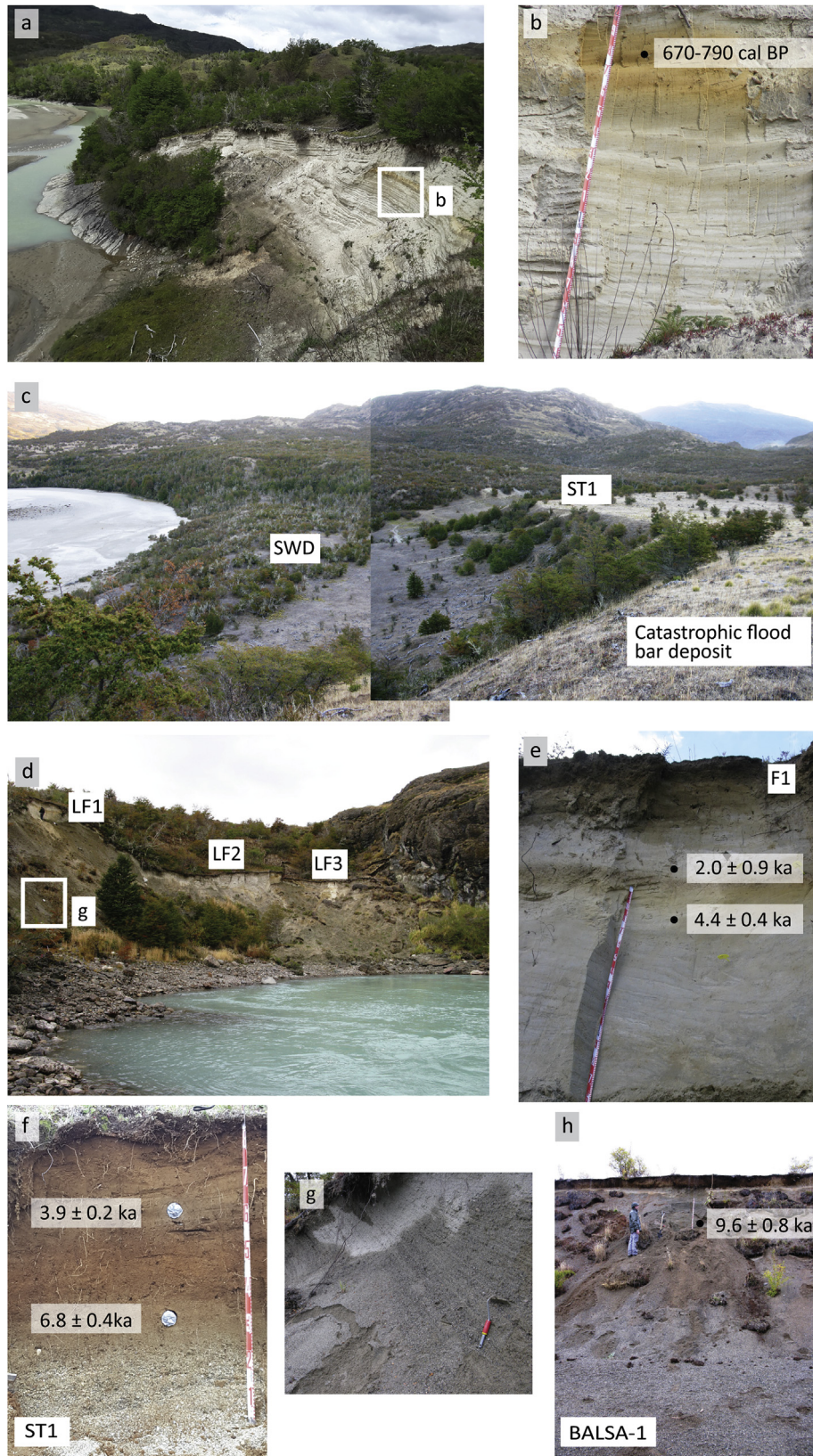


Fig. 6. Photographs from the Nef and Manzano study reaches. a) Downstream view of Nef River right bank section which preserves a sequence of 116 beds of Holocene SWDs. A flood-bed towards the base of the outcrop was OSL dated to 2.4 ± 0.1 ka. b) Detail of flood-beds at the Nef (NE) section consisting of fine sand and silt (4–16 cm thick) and a buried palaeosol with an *ante quem* radiocarbon age of 790–670 cal BP for a sequence of high magnitude flood-beds overlying the palaeosol. c) Composite view of the Baker valley at Manzano reach, with a staircase of fluvial surfaces formed by catastrophic flood bar deposits, fine gravel and sand GLOF deposits and SWDs. d) La Fortuna site with location of three flood benches at 23.5 m (LF1), 16.5 m (LF2) and 14.3 m (LF3) a.w.l. e) Sequence of 26 flood-beds below a reddish palaeosol, overlain by another 6 flood units (LF1 profile). f) Detail of two OSL dated flood-beds separated by a buried soil in the ST1 profile located ~30 m a.w.l. g) Detail of coarse sand and gravel deposits in d), showing large foresets dipping

Downstream of the La Fortuna site, on the right valley side, a valley embayment contains four sand benches, at elevations of 10 m, 17.5 m, 22 m and 25 m a.w.l (Fig. 6c). There are no outcrops exposing a complete stratigraphy, however, we note their comparable elevations to the La Fortuna sections, which suggests a similar relationship to flood magnitude and timing. A section of the upper bench (ST1) exposes two sandy flood-beds of SWD facies sitting above a cross-bedded gravel and coarse sand deposit interpreted as a megaflood-type flood landform (Fig. 6f). The two flood-beds were separated by a well-developed orange coloured palaeosol (Fig. 6f). The lower flood layer (14 cm thick), was OSL dated to 6.8 ± 0.4 ka, and is composed of graded coarse to medium sand. The upper flood unit (12 cm thick) comprises massive fine to very fine sand, light brown in colour, capped by a 20 cm thick orange-brown palaeosol. This upper flood-bed was OSL dated to 3.9 ± 0.2 ka and a charcoal sample from the upper palaeosol provided an age of 2465–2750 cal BP. Section ST5 consists of one flood sand bed (60 cm thick) with horizontal to wavy lamination, OSL dated to 6.4 ± 0.4 ka. The ST5 deposit is inset beneath the upper surface of a boulder-capped longitudinal bar, and is ~33 m above the river channel.

4.3.3. Baker–Colonia reach

This study reach is located upstream of a narrow bedrock control reach (Fig. 5c), which features an inner channel eroded by catastrophic flooding (Benito and Thorndycraft, 2020). Other megaflood-type landforms include boulder capped longitudinal bars, located upstream of a cross-valley dyke. These bars likely resulted from the moraine breach (flood event 3, Fig. 2) located at the Colonia-Baker confluence (Thorndycraft et al., 2019). Inset within the megaflood-type landforms are Holocene alluvial sediments and a group of aeolian dunes (Fig. 5c). The hydraulic control at the downstream end of the reach resulted in vertical accretion of alluvial sediments upstream to the Colonia junction. The sedimentology is therefore dominated by stacks of fine-grained flood-beds alternating with buried palaeosols. Upstream of the Colonia confluence, the floodplain is wider and dominated by lower elevation alluvial sediments with a greater control of lateral fluvial processes. Along the Baker-Colonia study reach, four main profiles were described (Figs. 5c and 9a).

The oldest (highest) alluvial benches, at La Valla (LV) and La Barca (LB), preserve the most complete flood record at this reach (Fig. 9a). The LV profile (3.5 m in thickness) contains basal gravels capped by a well-developed buried palaeosol (PS1) that was radiocarbon dated to 6940–7165 cal BP (Fig. 7a and b). Overlying this palaeosol are at least three major flood units (LV-01 to LV-03) that occurred between then and ~5940–6195 cal BP. These flood-beds are 20–25 cm thick, composed of white to greyish very fine sand to silt with ripples. Individual flood-beds contain yellowish brown edaphic features in the upper 10–15 cm, likely indicating low flood frequency at this time.

The mid-section of the profile comprises at least eight flood units (LV-04 to LV-11), varying in thickness from 5 to 25 cm, with the upper most flood-bed (LV-11) capped by a reddish palaeosol (PS2). These flood-beds are composed of fine to very fine, white to grey sand, with parallel lamination and ripples, and rip-up clasts, overlain by thin laminae of silt to clay. These eight flood units were deposited between ~5325–5585 cal BP and ~2490–2775 cal BP, the latter assuming a stratigraphic correlation with a similar Bw palaeosol horizon dated at the RA and LB profiles.

The upper most sequence contains at least two flood-beds (LV-

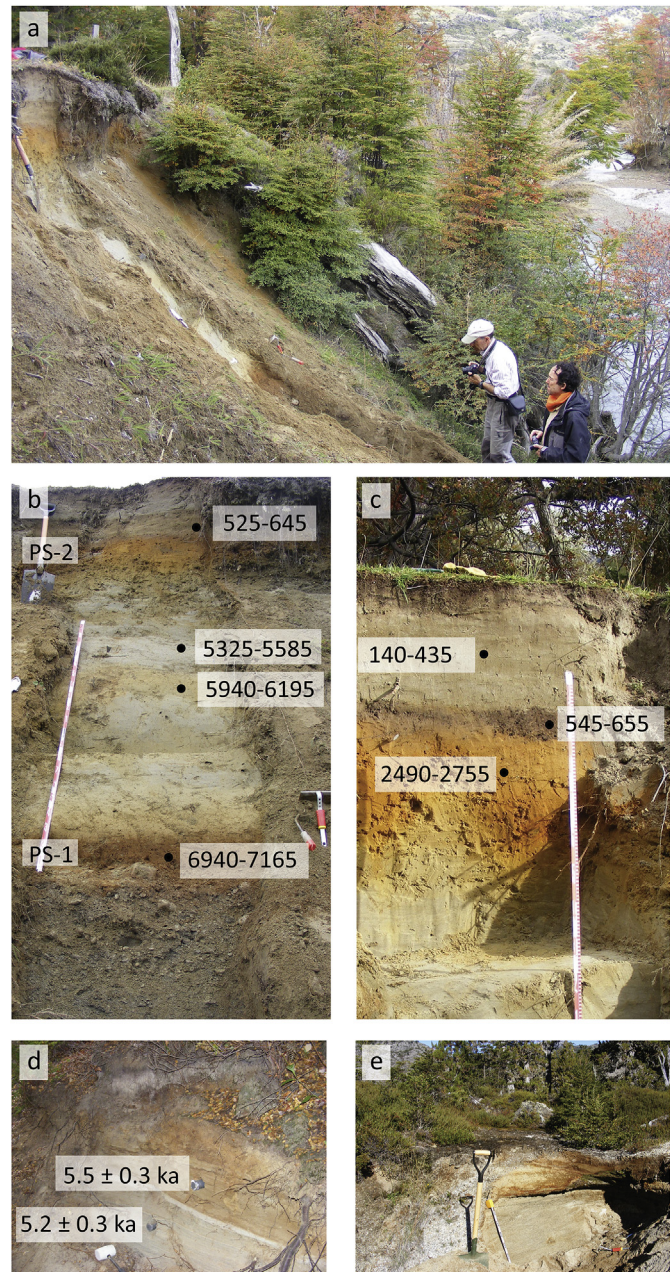
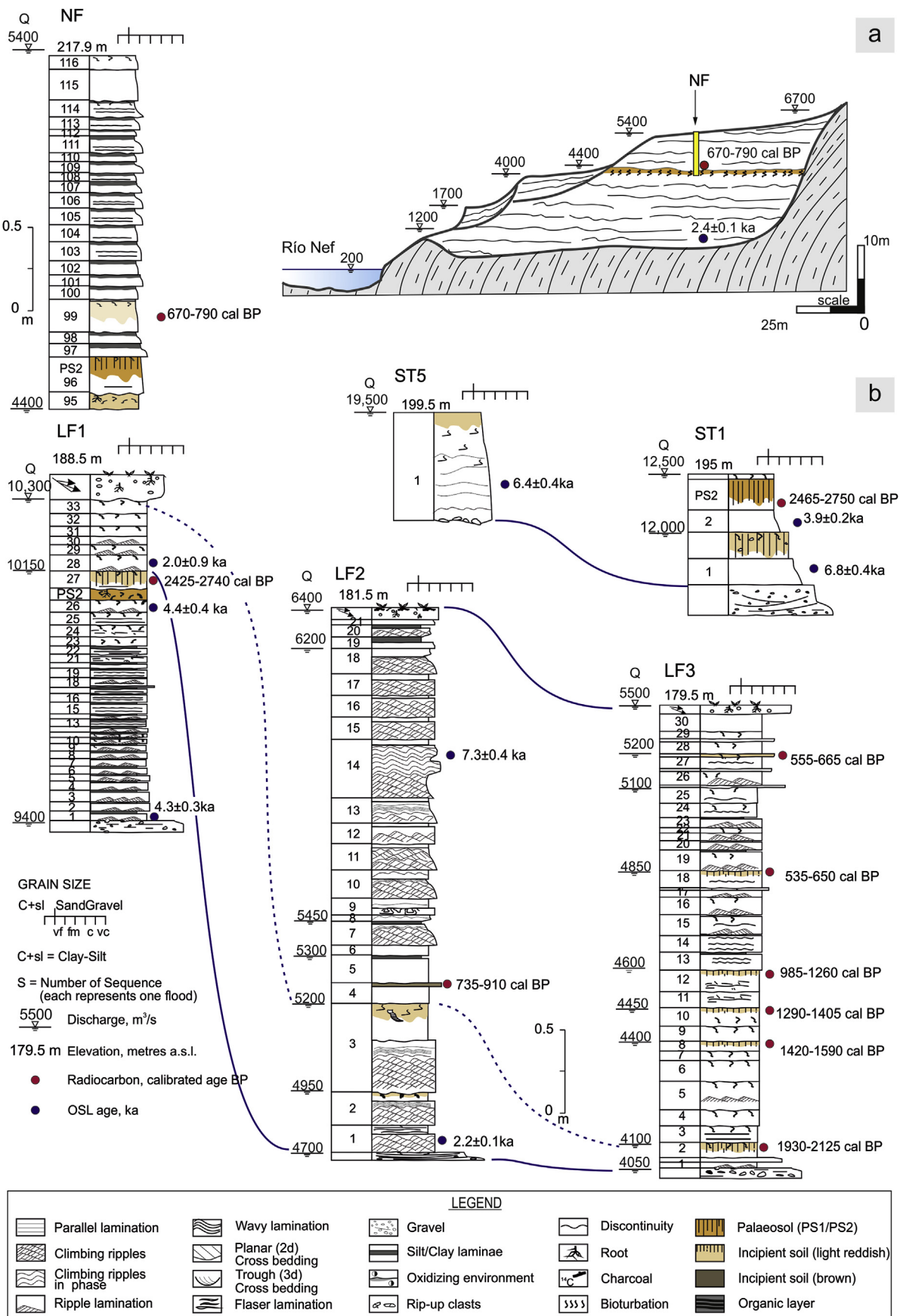


Fig. 7. Photographs from the Colonia and San Carlos-Vargas study reaches. a) Side view of the LV upper floodplain profile, shown in panel b). The site is +6.5 m a.w.l. - note a left bank branch of the Río Baker rejoins the main river in the background (flow away from the viewer). b) View of the LV profile, showing whitish flood sands above basal gravels. Note reddish/orange palaeosols indicating reduced flood inundation. Selected radiocarbon dates (cal BP) are shown. c) Detail of the upper LB profile, with a 0.4 m thick buried palaeosol (radiocarbon dates in cal BP). d) View of units 4 and 5, with OSL ages, at San Carlos profile with contact marked by white sand. e) Coarse sand at Vargas profile VA3, showing at least two flood-beds. The lower unit contains cross-bedding dipping towards the valley margins, and the upper one shows trough cross-stratification beds, likely formed during migration of megadune sets. (For interpretation of the references to colour in this figure legend, the reader is referred to the web version of this article.)

downstream deposited by the Baker-Bertrand catastrophic flood. This deposit occupies the inner channel indicating channel incision by the catastrophic flood (Benito and Thorndycraft, 2020), and were deposited during the later stages of the flood. h) Coarse sand and fine gravel beds deposited by the Baker-Bertrand catastrophic flood in an eddy environment located at Valle Grande (Fig. 2). The deposit was OSL dated to 9.6 ± 0.8 ka.



12 to LV-13), that inundated the upper alluvial terrace. These flood-beds, ~20 cm thick, are composed of fine sand with parallel lamination, LV-12 light brown in colour, and LV-13 whitish grey. Both flood-beds are capped by an incipient dark brown soil composed of 3–5 cm thick horizon of fine sand, silt and clay with bioturbation. Radiocarbon dating yielded an age of 525–645 cal BP (CE 1305–1425) for LV-12 and 135–310 cal BP (81% probability; CE 1640–1815) for LV-13.

At La Barca (LB), flood deposits accumulated on a 300–400 m wide alluvial terrace at 7 m a.w.l. on which another flood bench is inset at 4.6 m a.w.l. In the upper alluvial terrace, the stratigraphy shows a lower sequence of at least nine sandy flood-beds (LB-02 to LB-10) with parallel lamination. The upper flood-bed (LB-10) consists of a 1 m-thick sand unit with climbing ripples showing reverse flow direction. The upper 50 cm of this unit developed into a reddish brown B soil horizon (PS2) dated to 2490–2775 cal BP (Fig. 7c).

The upper sequence comprises of at least three identifiable flood-beds (LB-11 to LB-13). The lower flood-bed (LB-11) was radiocarbon dated to 545–655 cal BP (CE 1295–1405). LB-12 is a 45 cm thick light grey medium to fine sand exhibiting parallel lamination that contains charcoal dated to 140–435 cal BP (89.5% probability within CE 1515–1810). The upper flood-bed (LB-13) consists of 4 cm thick light grey sand with parallel lamination dated to 10–270 cal BP (CE 1680–1940).

Further upstream, the Raices (RA) profile (opposite the Colonia confluence), comprises two main sediment stacks. In the lower section we identified at least four flood-beds of light reddish sandy silt, with RA-02 radiocarbon dated to 2430–2725 cal BP. This flood date is consistent with the termini of the lower flood sequence dated in La Barca. The upper stack includes at least eleven flood-beds deposited over the last 550 years, based on a radiocarbon date of 490–545 cal BP from flood-bed RA-07. The upper most three flood-beds (RA-13 to RA-15) post-date a radiocarbon date of CE 1957 (104.47 ± 0.34 pMC).

Downstream, the undated La Playa (LP) profile (Fig. 4c) shows a similar two phase stratigraphy to the RA profile. Here, the lower stack comprises eleven flood units of an orangey silty sand, with the upper flood-bed (PL-01 to PL-11) showing remnants of a truncated red brown palaeosol, characteristic of the termini of the Mid to Late Holocene fluvial sequence (see proposed stratigraphic correlation on Fig. 9a). Overlying an unconformity, we identified at least 15 flood-beds in the upper stack (PL-15 to PL-26). These were composed of fine to medium well sorted sand with light brown colour.

4.3.4. San Carlos-Vargas reach

The SC profile occurs ~2 km downstream of the San Carlos narrows (Fig. 5d), a short gorge section of the Río Baker featuring an eroded inner channel formed by catastrophic flooding (Benito and Thorndycraft, 2020). A prominent megaflood-type landform feature of the reach is a flood-scoured lake with downstream longitudinal bar, formed when floodwaters crossed a col in a bedrock spur. Downstream of the lake and in the lee of the bedrock spur, a 15 m high bar was deposited. We interpret this as a composite landform, formed by catastrophic flooding, but overlain by later flood-beds. A trail cut exposes a 2.2 m thick stratigraphic section comprising at least five sand-to-fine gravel flood-beds with planar and trough cross-bedding (15 cm high 3D dunes), each flood-bed separated by unconformities or laminated silts. SC-04 comprises 45 cm of white to greyish medium to coarse sands with planar

cross-bedding and parallel lamination (Figs. 7d and 9b). This unit was OSL dated to 5.2 ± 0.3 ka. Overlying a 3-cm thick ash-grey coloured silt, SC-05 (dated to 5.5 ± 0.3 ka) consists of medium to coarse reddish sand with sub-horizontal to wavy lamination. This flood stack is capped by a palaeosol with an organic A horizon and mollic epipedon, a 10 cm thick layer of loose whitish massive sand and silt, and a 7 cm thick light brown fine to medium sand. The fluvial origin of these two sand layers is uncertain and they could be deposited by aeolian processes.

We described the flood stratigraphy ~22 km downstream at a site of valley expansion separating the Baker and Vargas valleys (Fig. 2, inset). This drainage divide (10 m a.w.l.) contains erosional and depositional landforms formed by catastrophic flooding, at present occupied by wetlands. Four Vargas profiles (VA1–VA4; Fig. 9b) from shallow quarry sites show at least three flood units made of fine gravel and coarse sand exhibiting cross-bedding and ripples in fining up sequences (Fig. 7e). We were unable to obtain age control on these flood-beds.

4.4. Flood modelling and estimation of flood magnitude

Discharge estimates using hydraulic flood modelling rely on the assumption that the elevation of a flood-bed was close to maximum stage attained during the event. The flood geomorphology of our four study reaches along the Baker River (Fig. 2) provide contrasting settings with respect to flood-bed elevation, flood stage and peak discharge relationships. The accommodation space at the Nef site, upstream of the Baker-Nef confluence gorge (Fig. 4a), has allowed accumulation of almost 15 m of flood sediments so is an example of a self-censored flood stack (cf. House et al., 2002), where progressive vertical accretion of sediments on the flood bench means progressively higher discharges are required to deposit a new flood-bed. There is a smaller accommodation space at the La Fortuna site (Manzano reach, Fig. 4b), located within a narrow gorge reach incised by the Bertrand-Baker catastrophic flood (Benito and Thorndycraft, 2020). Here, in a zone of eddy circulation, three flood sediment stacks are preserved at bench elevations of 23.5 m (LF1), 16.5 m (LF2) and 14 m (LF3) above the river channel creating a flood record sensitive to variations in flood stage and, therefore, magnitude (Fig. 10). The Colonia-Baker reach features a stable alluvial terrace accumulated upstream from a catastrophic flood-carved control section (Fig. 4c). The occurrence of overbank fine grained flood-beds and repetition of buried soils along high (>5 m) river bank sections demonstrate vertical accretion processes along the reach. The sediments are not as thick as in the Nef reach but there is vertical self-censoring of the palaeodischarge record, and only large magnitude floods could inundate the youngest palaeosols. At San Carlos, Mid-Holocene flood sediments were deposited on top of a catastrophic flood eddy bar, on the inside of a bend in the valley (Fig. 4d). Sedimentation occurred from secondary flow circulation, near the flow separation point, and 12 m above the valley floor, so the section only preserves high magnitude floods. At the Vargas sites (VA1–VA4) flood stage exceeded a threshold of ~10 m a.w.l. To synthesise the palaeodischarge records at the four reaches, in general the flood stacks at the Manzano and San Carlos sites are more sensitive as recorders of extreme flood discharges throughout the Holocene, while self-censoring at the Nef and Colonia sites means interpretations on extreme floods are more robust over the last millennia.

Fig. 8. a) Stratigraphic profile for the upper sequence of flood-beds, and a schematic cross-section, showing the position of the NF profile, for the Nef site. (b) Stratigraphic profiles and proposed correlations for the study sections at El Manzano. Site labels refer to locations in Fig. 5. Altitudes at the top of the sections were determined from field surveys supported by 1:10,000 scale topographic maps and are in meters above sea level (m a.s.l.). Discharge values refer to the indicated flow stage computed by hydraulic modelling described in Section 4.4. Radiocarbon dates in calibrated years BP (2σ) and optically stimulated luminescence (OSL) dates in ka.

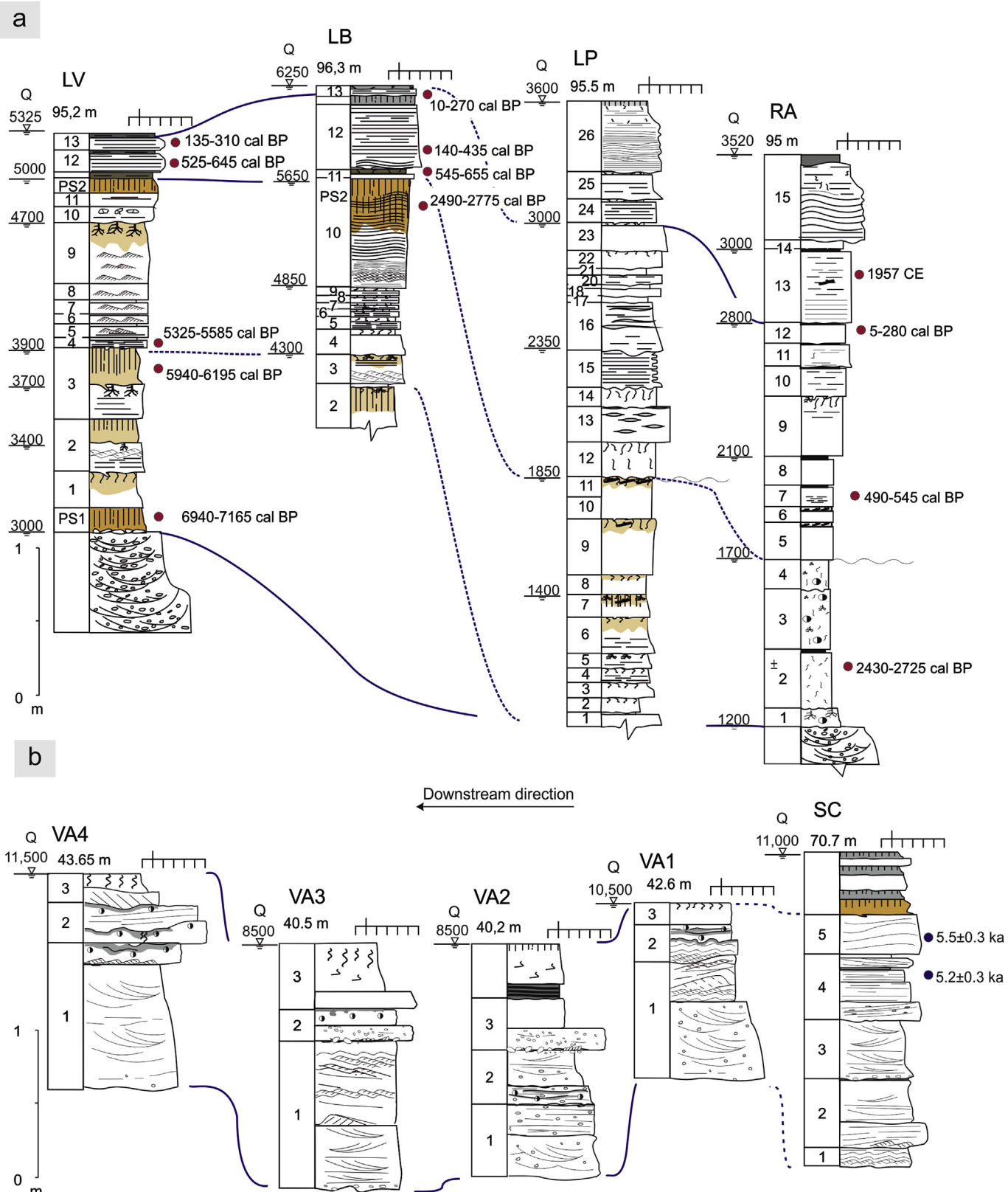


Fig. 9. Stratigraphic profiles and proposed correlations in the Colonia (a) and San Carlos-Vargas (b) sites. Site labels refer to locations in Fig. 5. Altitudes of tops of described sections at the Colonia sites were determined from differential GPS survey, and in San Carlos-Vargas sites from field surveys supported by 1:10,000 scale topographic maps and are in meters above sea level (m a.s.l.). Discharge values refer to the indicated flow stage computed by hydraulic modelling described in Section 4.4. Radiocarbon dates in calibrated years BP (2σ) and optically stimulated luminescence (OSL) dates in ka. See Fig. 8 for legend.

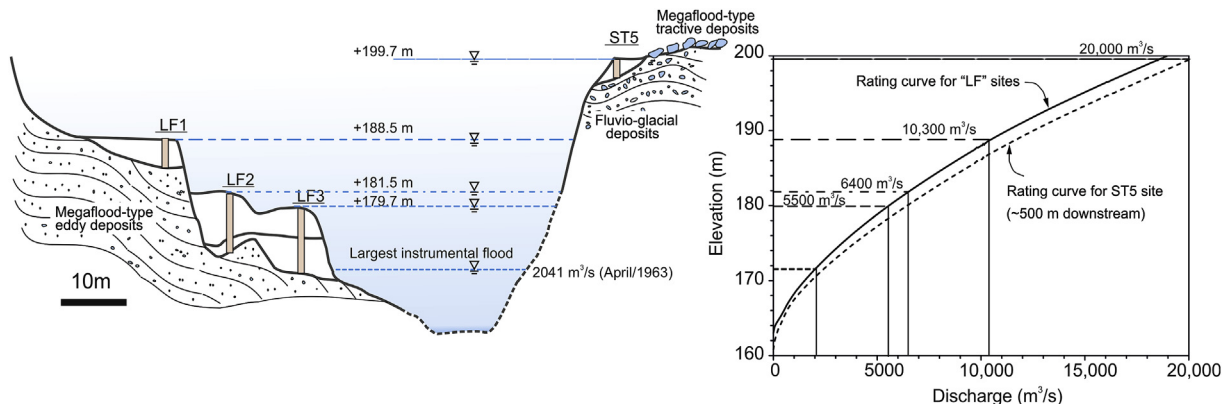


Fig. 10. Cross-section at the Baker-Manzano reach illustrating the location of SWDs at the La Fortuna benches (LF1 to LF3) and at ST5 site (~500 m downstream), shown alongside the modelled rating curves used to compute palaeoflood discharges. Note the stage of the maximum recorded flood at the Angostura Chacabuco station since 1963, and the high elevation reached by mid-Holocene floods at ST5 in relation to later floods at LF1-LF3 sites.

4.4.1. Nef

Due to the 15 m thickness of the sediment stack at the lower Nef site, the sequence of 116 flood units were deposited under a wide range of minimum flow discharges from 200 to 6700 m³/s. From the stratigraphy we have divided the sequence in to two sets (Fig. 8a). A lower sequence of 96 flood-beds, dating from 2.4 ± 0.1 ka were inundated by floods ranging from 200 to 4400 m³/s, so this record likely preserves rain-on-snow and snowmelt floods as well as GLOFs. This part of the sequence is the most affected by self-censoring with progressively higher elevation flood-beds requiring greater discharges to deposit new flood sediments so we do not consider these flood-beds in our composite GLOF inventory. The base of Set 2 of the sequence is marked by a palaeosol, which indicates a period of non-exceedance, with no floods above a threshold of ~4400 m³/s. A radiocarbon date of 670–790 cal BP was obtained for a flood-bed 40 cm above this palaeosol, providing a minimum age estimate for a sequence of 20 flood-beds with a discharge range of 4400–6700 m³/s.

4.4.2. Baker-Manzano

Eddy bar deposits at the Baker-Manzano reach were the most effective palaeostage indicators for determining minimum peak discharge of the catastrophic Bertrand-Baker flood, dated herein to 9.6 ± 0.8 ka (Section 4.1). Modelling resulted in a minimum peak discharge of 110,000 m³/s required to flood the eddy bars (Benito and Thorndycraft, 2020). The next largest flood magnitude was constrained by a range of discharges of 15,800–20,000 m³/s needed to overtop flood-beds at sites ST1 and ST5, dated to 6.8 ± 0.4 ka and 6.4 ± 0.4 ka respectively (Figs. 10 and 11a). At ST5, the upper palaeosol was radiocarbon dated to 2465–2750 cal BP, and this marks non-exceedance of floods reaching 20,000 m³/s over at least the last two millennia.

The range of minimum discharges required to flood the three stacks of flood sediments deposited from 4.3 ± 0.3 ka to ~555 cal BP at La Fortuna were: 9100–10,300 m³/s (LF1), 4700–6400 m³/s (LF2) and 4300–5500 m³/s (LF3). These discharges can be compared to the largest flood (April, 1963) recorded at the Angostura Chacabuco gauge station of 2041 m³/s (Figs. 10 and 11a). Evidence of modern flood sediment deposition is found at the right margin, upstream of El Molino stream junction, on the lowest flood bench (Fig. 5b), with modelled minimum discharges 1100–1700 m³/s required to flood these sediments located up to 2.5 m above the water level.

4.4.3. Baker-Colonia

At this reach, eroded scarps on the incised moraine at the upper end of the reach matched the discharge estimate of 110,000 m³/s for the Bertrand-Baker catastrophic flood (Benito and Thorndycraft, 2020). The next largest floods, with preserved geomorphic evidence, were associated with the three flood-beds deposited over the last 655 cal BP (LB-11 to LB-13), which post-dated the prominent buried palaeosol we mapped along the reach, dated to 2490–2775 cal BP. Minimum discharges of 5700–6250 m³/s were required to form these flood-beds (Fig. 11b). The palaeodischarges associated with older flood-beds, such as LV-04 to LV-11 post-dating 5325–5585 cal BP (LV-04), were likely more influenced by self-censoring, nevertheless modelling resulted in lower bound discharge estimates of 3900–5000 m³/s for this phase of flooding, higher than floods of the instrumental record (Fig. 3). The stratigraphy of the lowest (RA profile) flood bench (Fig. 9a) preserves a more complete record of recent floods ranging from 1700 to 3520 m³/s. Discharge estimates of eight flood-beds (RA-05 to RA-12), dated to ~0.5 ka according to a date of 490–545 cal BP (RA-07) range between 1700 and 2800 m³/s. The upper three flood-beds, corresponding to modern events post-dating 1957, were deposited from floods with minimum discharges of 3000–3520 m³/s. A large outburst flood from Lago Arco (Colonia valley) occurred in April 1958, reported by settlers as bigger than the ones recorded in the gauge station (1964 onwards), which is likely recorded in the stratigraphy ($Q > 3000$ m³/s). A sequence of five outburst floods in the Colonia Valley occurred in 1960s either from the Arco or Cachet tributaries (Dussaillant et al., 2010). The first one in April 1963 reported by settlers (Julio Romero Castro interviewed in 2010) has an unknown magnitude. The gauged outburst floods in Mar 1965 (2586 m³/s) and Jan 1967 (2770 m³/s) were smaller than those in Jan 1964 (3240 m³/s) and Mar 1966 (3089 m³/s), meaning that only two exceeded the RA-13 minimum discharge ($Q > 3000$ m³/s). Recent flooding from Lago Cachet II, with a range of recorded discharges of 2000 and ~3800 m³/s (Dussaillant et al., 2012; Jacquet et al., 2017) flooded the RA flood bench but failed to inundate the LV and LB floodplain surfaces. Note that the RA stratigraphy was described in April 2011 meaning that only the March 2009 flood ($Q > 3812$ m³/s) surpassed the RA-15 bed elevation ($Q > 3520$ m³/s).

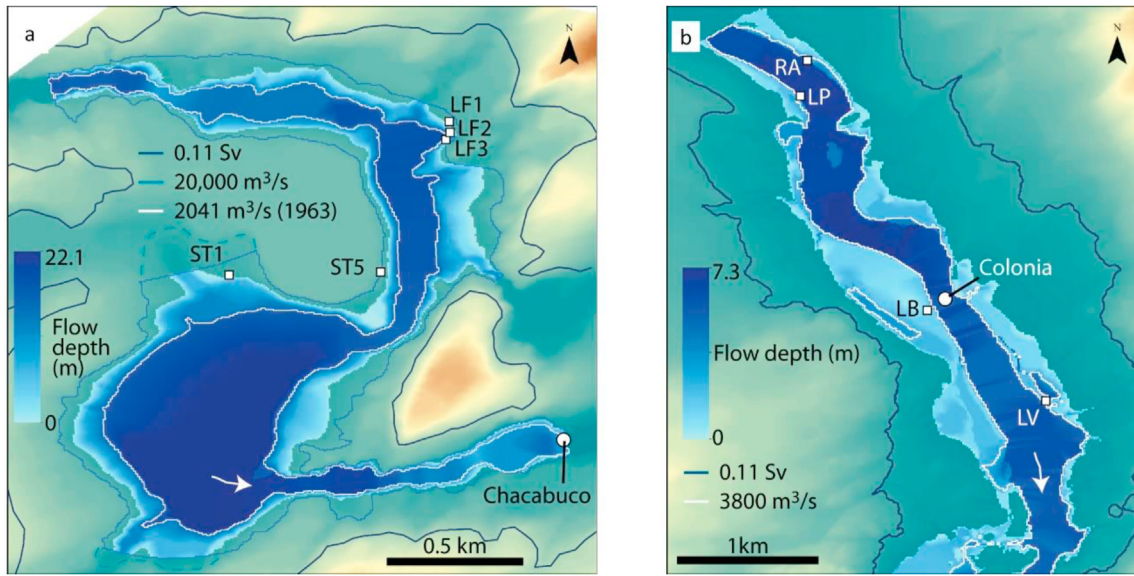


Fig. 11. Computed flood water depth for selected palaeoflood discharges at: a) the Baker-Manzano sector ($10,300 \text{ m}^3/\text{s}$) and b) the Baker-Colonia sector ($6250 \text{ m}^3/\text{s}$). The dark blue line in both panels shows the flow extent for the modelled Bertrand-Baker flow of $110,000 \text{ m}^3/\text{s}$ (0.1 Sv). The largest gauged floods since 1960 are illustrated by the white lines. The largest mid-Holocene flood extent at the Colonia reach ($20,000 \text{ m}^3/\text{s}$), matching the elevation of the ST5 deposits, is also presented in a). Note the dashed line for the $20,000 \text{ m}^3/\text{s}$ discharge shows the hypothesised flood extent beyond the edge of the one-dimensional model domain. (For interpretation of the references to colour in this figure legend, the reader is referred to the web version of this article.)

4.4.4. San Carlos-Vargas

At San Carlos, one sedimentary section was described. Here the stack of eddy flood sediments, dated to $5.5 \pm 0.3 \text{ ka}$ and $5.2 \pm 0.3 \text{ ka}$, are associated with modelled lower bound discharges of $10,630\text{--}11,000 \text{ m}^3/\text{s}$ (Fig. 9b). At ca. 22 km downstream of San Carlos, these floods overflowed the water divide with the Río Vargas currently occupied by wetlands that required a threshold discharge of $8500\text{--}11,500 \text{ m}^3/\text{s}$ (Fig. 9b).

5. Discussion

5.1. Baker valley composite GLOF record and Holocene neoglacials

Here we synthesise the palaeoflood discharge and timing record from the multiple stratigraphic sections across the study reaches in order to develop a composite, long-term GLOF magnitude and frequency record for the Baker valley (Fig. 12). We assign palaeo-GLOF events based on a threshold discharge of $3000 \text{ m}^3/\text{s}$, $\sim 500 \text{ m}^3/\text{s}$ greater than the largest modern rainfall or snowmelt floods recorded in the instrumental data series (Fig. 3). This means that at the Nef site, for example, we discount, from the composite record, the lower sequence of 96 flood-beds, dated between $2.4 \pm 0.1 \text{ ka}$ and $670\text{--}790 \text{ cal BP}$. Some of the uppermost flood-beds in the lower sequence do exceed $3000 \text{ m}^3/\text{s}$ however, given uncertainty on timing, these have not been included in the composite record. The upper sequence of 18 floods (NE-99 to NE-116), post-dating the $670\text{--}790 \text{ cal BP}$ flood-bed and exceeding a threshold discharge of $4400 \text{ m}^3/\text{s}$, were assigned as GLOFs. We also consider the possibility of floods being repeated at downstream sites, so for example the 18 floods (NE-99 to NE-116) above $4400 \text{ m}^3/\text{s}$ closely matches the La Fortuna LF3 record of 19 floods (LF3-12 to LF3-30), which post-dated $985\text{--}1260 \text{ cal BP}$ and exceeded flows of $4500 \text{ m}^3/\text{s}$ - so only one additional event from LF3 was added to the composite record.

In total we identify a minimum of 86 outburst flood events spanning the last 10 ka in the Baker valley. The discharge (magnitude) and timing of these individual events are presented on

Fig. 12. In Fig. 13, these events are grouped into six GLOF phases and compared to the Holocene neoglacials of the PATICE record (Davies et al., 2020). GP-1 is characterised by high magnitude floods ($\sim 1 \times 10^5 \text{ m}^3/\text{s}$), associated with ice recession at the end of the Last Glacial Interglacial Transition (Fig. 13). The floods during this phase include drainage of Lago Chelenko (Thorndycraft et al., 2019). This likely breached in the lower Baker (No. 1, Fig. 1), and to date no flood reconstruction has been attempted given remote access and a wide and forested lower Baker valley, however a Bayesian age model using *ante* and *post quem* dates constrains drainage to $12.4\text{--}11.8 \text{ ka}$ (Thorndycraft et al., 2019). This timing post-dates ice recession following the Antarctic Cold Reversal and pre-dates likely ice stabilisation $\sim 11 \text{ ka}$ (Glasser et al., 2012; Davies et al., 2020). The drainage of Lago Chelenko resulted in the formation of multiple moraine and ice dammed lakes, which drained during at least three separate GLOF events from lakes Colonia, Cochrane and General Carrera/Buenos Aires, releasing 9 km^3 , 37 km^3 and 94 km^3 of water respectively (Thorndycraft et al., 2019). Chronologically, the first catastrophic drainage corresponded to Lago Colonia impounded by a moraine at the Baker-Colonia junction with a spillway at $\sim 145\text{--}150 \text{ m a.s.l.}$ (Thorndycraft et al., 2019) (Fig. 2; Site 3). The drainage from Lago Cochrane/Pueyrredón also demonstrates characteristics of high magnitude outburst flood with boulder bar deposits at the lake outlet (Fig. 2; Site 2). The Bertrand-Baker flood is well constrained both in terms of timing ($9.6 \pm 0.8 \text{ ka}$, this study), post-dating the 11.0 ka ice stabilisation (Davies et al., 2020), and discharge ($110,000 \text{ m}^3/\text{s}$; Fig. 2; Site 5), which was constrained by ubiquitous erosional and depositional evidence left along the flood pathway (Benito and Thorndycraft, 2020). Other floods in the upper Baker catchment include palaeolake Tranquilo (Martin et al., 2019) draining into Valle Grande (Fig. 2; Site 4). This phase (GP-1) was followed by the formation of a palaeosol (PS1, Fig. 12), dated at the LV profile to $6940\text{--}7165 \text{ cal BP}$, suggesting limited flood exceedance ($>3000 \text{ m}^3/\text{s}$) at this time.

GLOF Phases GP-2 and GP-3 are associated with a Mid-Holocene neoglacial (Fig. 13) constrained to $6\text{--}4 \text{ ka}$ (Davies et al., 2020). Evidence for moraine formation in the Baker basin at this time

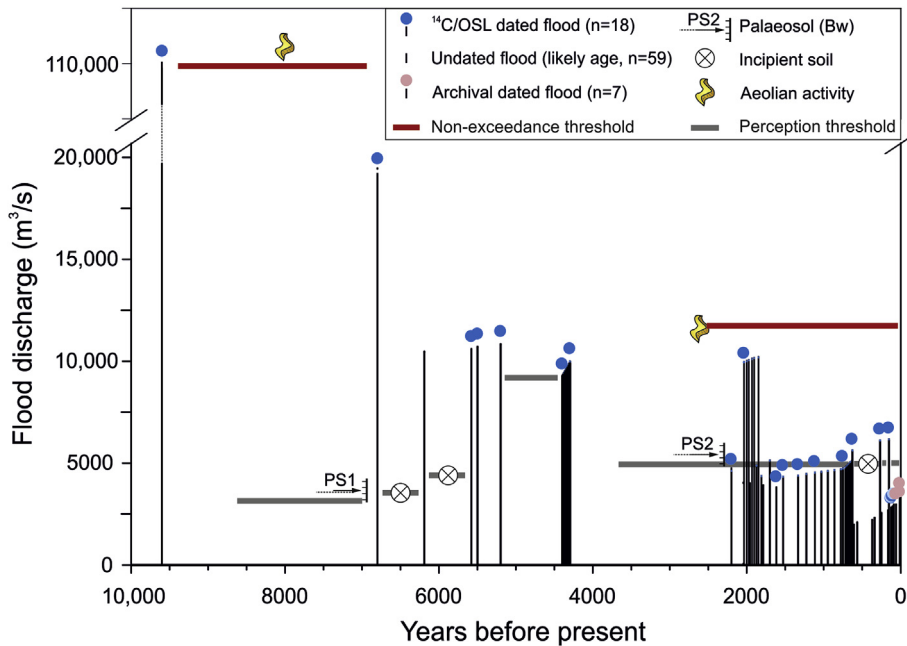


Fig. 12. Temporal GLOF distribution and quantified discharges for the Baker catchment during the Holocene. Each bar represents a single GLOF event. Note the discharge axis was broken at high discharges to include the Bertrand-Baker catastrophic flood with a modelled flow of $110,000 \text{ m}^3/\text{s}$ (0.11 Sv). The dated floods and known GLOF dates from observational records (archival and instrumental) are highlighted with circles. Timing of undated GLOFs was interpreted based on their stratigraphic position bracketed by dated flood-beds. The temporal distribution of the main palaeosol phases (PS1 and PS2), incipient soil development (ochric horizons) and aeolian activity are shown – these being indicators of flood non-exceedance.

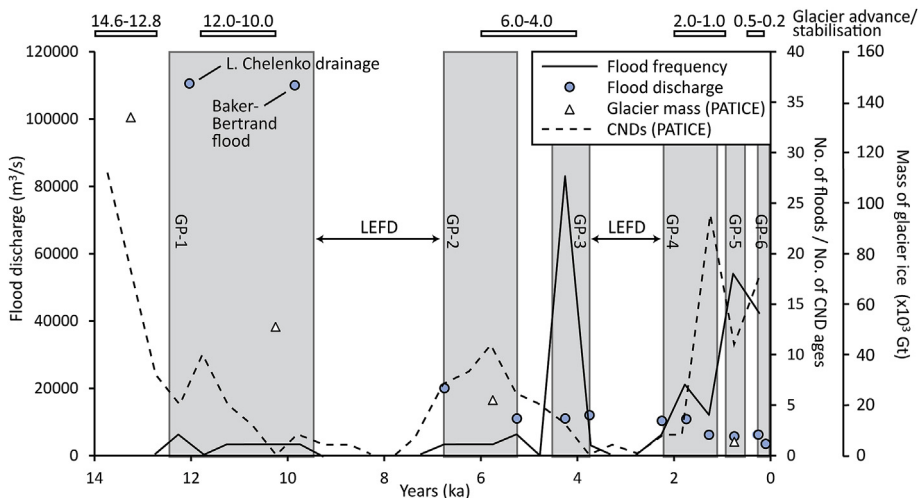


Fig. 13. GLOF flood magnitude (discharge) and frequency, and timing of Holocene neoglacials (number of dated CND samples per 500 year bin, included in the PATICE database, Davies et al., 2020). Also shown is the mass of glacier ice for the Patagonian ice-sheet (Davies et al., 2020). GLOF frequency is indicated by the number of floods per 500 year bin. The inferred GLOF phases (GP) and periods of low extreme flood frequency (LEFD) are illustrated. GLOF magnitude is the largest, dated, discharge estimated for a flood within the 500 year bin, and the largest instrumental GLOF discharge. The timing of Lago Chelenko drainage is also shown. Note, there has been no discharge estimation for this event but based on the elevation of raised deltas and the areal extent of Lago Chelenko we infer the discharge to be in the order of 0.1 Sv, but likely larger than the Bertrand-Baker flood given the greater volume of water drained (Thorndycraft et al., 2019).

includes the moraine damming Lago Colonia (Fig. 2), which was dated to 4.96 ± 0.21 ka by Nimick et al. (2016), the age standardized to 5.4 ka (0.2 standard deviation) in the PATICE database (Davies et al., 2020). Similar ages were obtained from moraines of the Monte San Lorenzo ice-cap in the southeast of the Baker catchment (Fig. 2). Here, a PATICE standardized mean age of 5.7 ka (0.1 standard deviation) was calculated for the Tranquilo Glacier (Sagredo et al., 2016).

GP-2 features five palaeoflood events exceeding $10,000 \text{ m}^3/\text{s}$

(Fig. 12). One event preserved at the Manzano reach (ST5) was dated to 6.8 ± 0.8 ka with a modelled discharge of $\sim 20,000 \text{ m}^3/\text{s}$. This phase ends ~ 5.5 ka, so early in the 6–4 ka neoglacial, with the evidence for at least two events exceeding $\sim 11,000 \text{ m}^3/\text{s}$ at San Carlos. We infer that these floods are likely those preserved at Vargas in the undated stratigraphic profiles, based on the need for threshold discharges $>8500 \text{ m}^3/\text{s}$ to flood the wide valley floor at this locality, and the coarser sediment size compared to the LF1 profile with a comparable threshold discharge.

GP-3 is notable for the highest flood frequency in our Holocene flood record (Fig. 13). A series of 26 flood-beds preserved in the highest elevation Fortuna flood stack (LF1-01 to LF1-26) were constrained by a lower age of 4.3 ± 0.3 ka and upper age of 4.4 ± 0.4 ka (Fig. 12), occurring during the final stages of the 6–4 ka neoglacial (Davies et al., 2020). These floods are associated with lower bound discharges of 10,000 to 11,000 m^3/s . Stratigraphic evidence for a higher flood frequency at this time is the lack of incipient palaeosol development compared to the lower benches (LF2 and LF3) preserving later flood deposition at the La Fortuna site. Modern analogues for this flood-bed sequence is found in the multiple outburst floods of the Cachet II and Arco lakes, both formed in ice dammed tributaries of the Colonia valley when tributary glaciers receded and decoupled from the Colonia glacier (Nimick et al., 2016; Jacquet et al., 2017). There were at least 15 known flood events from Lago Arco during the period 1881–1967 (Tanaka, 1980; Harrison and Winchester, 2000) and 27 floods from Cachet II between 2008 and 2017. We infer, therefore, that the 26 flood-beds preserved at LF1 were a sequence of ice-dammed GLOFs occurring at the end of the 6.0–4.0 ka neoglacial (Fig. 13) likely during a period of glacier instability. To summarise GP-2 and GP-3, therefore, a phase of high magnitude but low frequency events likely occurred at the start of the neoglacial, with high frequency of ice-dammed GLOFs at the end.

Following the 6–4 ka neoglacial there is a period of low extreme flood frequency in the Baker palaeoflood record. The stratigraphy of LF1, including the development of palaeosol PS2 dated to 2425–2740 cal BP, suggests non-exceedance of floods $>10,000 \text{ m}^3/\text{s}$ for ~2000 years from ~4.0–2.0 ka. The source bordering dune at the Manzano reach (Fig. 2) was dated to this period (2.6 ± 0.2 ka) and provides evidence for non-exceedance of floods $>12,000 \text{ m}^3/\text{s}$ over the last three millennia (Fig. 12), meaning that floods LF1-28 to LF1-33 can be constrained to 10,000–12,000 m^3/s in magnitude. However, we note that at the Colonia reach, non-exceedance associated with the PS2 palaeosol (dated to 2490–2775 cal BP at the LB profile) lasted until ~0.7 ka without floods $>5000 \text{ m}^3/\text{s}$.

The upper flood-beds of LF1, dated to 2.0 ± 0.9 , and a sequence of 12 flood-beds preserved at LF3, dated between 1930 and 2125 cal BP and 985–1260 cal BP, marks GP-4 and coincides with the 2.0–1.0 ka neoglacial (Davies et al., 2020). In the Baker catchment, Harrison et al. (2007) used both cosmogenic nuclide exposure dating and OSL to date a Leones Glacier moraine to 1.1 ± 0.2 ka (Davies et al., 2020) and Glasser et al. (2002) reported a readvance of Soler Glacier at 1222–1342 CE. The range of flood discharges for the LF3 events are 4050–4600 m^3/s , but at least six events, post-dating 2.0 ± 0.9 ka, had higher discharges of 10,150–10,300 m^3/s and exceeded the PS2 palaeosol at LF1 (LF1-28 to LF1-33). We infer the LF1-28 to LF1-33 flood-beds date to the initial stage of the neoglacial during a short-time period (likely predating flood-bed LF3-02), meaning a frequency of one event every 26 years. The later LF3 sequence over this 900 year period contains four incipient palaeosols indicating a phase of relatively low flood frequency (one event every ~160 years) during GP-4. This phase of flooding is not recorded at the Colonia site.

GP-5 begins at ~0.7 ka. This phase includes the LF3 flood-beds (LF3-13 to LF3-27) post-dating the end of GP-4 at 985–1260 cal BP, with the latter 10 floods bracketed by overlapping ages of 535–650 cal BP and 555–665 cal BP suggesting a possible cyclical phase of ice-dam failures. These floods post-date the 2.0–1.0 ka PATICE neoglacial, and marginally pre-date the last Holocene neoglacial at 0.5–0.2 ka (Davies et al., 2020). Minimum palaeodischarges at this time range from 4600 to 5700 m^3/s at the LF3 site. These floods coincided with the flood-beds from the upper sequence of the Nef profile. Here three flood-beds are preserved from PS2 to the incipient palaeosol dated to 670–790 cal BP,

suggesting a low flood frequency coinciding with the 2.0–1.0 neoglacial (Fig. 13), prior to a sequence of 18 floods (4500–5400 m^3/s) post-dating 670–790 cal BP. At Colonia, an individual large magnitude flood (5000–5600 m^3/s) was dated to 525–645 cal BP at LV, and to 545–655 cal BP at the LB profile, and we interpret this as a moraine dam GLOF. To summarise the GP-4 and GP-5 phases, there appears to be a period of low flood frequency coinciding with the 2.0–1.0 ka neoglacial, and increased flood frequency at ~0.7–0.6 ka pre-dating the 0.5–0.2 ka neoglacial. GP-5 is coincident with a period of increased flood frequency recorded in Valle Grande from 0.75 to 0 cal kyr BP (Vandekerhove et al., 2020).

The final flood phase (GP-6) is represented by the youngest flood-beds dated at the Colonia reach. Two floods at La Barca (LB) and La Valla (LV) (dated to 135–310 cal BP and 10–270 cal BP, respectively) exceeded 6200 m^3/s , otherwise the 12 floods preserved at the lower elevation Raices (RA) and Playa (LP) sites exceed discharges of 2100–3520 m^3/s . These floods are associated with the end of the last neoglacial. Dendrochronology was used to date a Nef Glacier moraine crest to 1863 CE (Winchester and Harrison, 2000), and at Lago Arco to 1881 CE when Arco lake reached its maximum level (Harrison and Winchester, 2000) (Fig. 2). It is likely that the Raices and Playa sites record some of the known 15 GLOFs that occurred between 1881 and 1967 from the Arco tributary of the Colonia Glacier (Harrison and Winchester, 2000; Tanaka, 1980). Indeed the RA-13 flood-bed ($Q > 3000 \text{ m}^3/\text{s}$) was radiocarbon dated to 1957 CE so could be one of the large subsequent GLOFs that occurred in Jan 1958 (unknown Q), Apr 1963 (unknown Q), Jan 1964 (3240 m^3/s) and Mar 1966 (3089 m^3/s). There is no dating evidence for floods of this magnitude at the Manzano study reach suggesting GLOFs at this time were likely sourced from the Colonia valley and not the Nef.

5.2. Declining GLOF magnitudes through the Holocene

The Holocene GLOF record from the Baker valley provides a long-term, empirical palaeodischarge dataset spanning ~10,000 years. The data show declining flood magnitude following the catastrophic 0.1 Sv Bertrand-Baker flood, dated to 9.6 ± 0.8 ka, falling to 0.001 Sv for the modern Cachet II GLOFs, recorded by the Río Baker gauge station at Colonia (Fig. 12). The largest palaeoflood event of the last millennia reached 6200 m^3/s , but generally the floods ranged between 3500 and 5700 m^3/s during the GP-5 and GP-6 flood phases. Minimum flood discharges were generally higher from ~7.0 ka to 1.5 ka (spanning GP-2 to GP-4), with the ST5, ST1, San Carlos and La Fortuna LF1 flood-beds all requiring threshold discharges of 10,000–20,000 m^3/s (0.01 Sv).

While individual glacier floods can relate to a wide range of physiographic settings, and GLOFs may be triggered by breaching of ice or moraine dammed lakes, the decline in flood magnitude through the Holocene broadly corresponds to a fall in ice sheet mass (Fig. 13), based on the PATICE reconstruction of total Patagonian glacier ice mass (Davies et al., 2020). Davies et al. (2020) reconstructed an ice sheet mass of $134.2 \times 10^3 \text{ Gt}$ at the end of the Antarctic Cold Reversal (13 ka). Warming from ~12.8 ka resulted in ice mass loss to $51.0 \times 10^3 \text{ Gt}$ by 10 ka, $21.7 \times 10^3 \text{ Gt}$ at 5 ka and $5.5 \times 10^3 \text{ Gt}$ during the last neoglacial (0.5–0.2 ka; Fig. 13). The Río Baker palaeodischarge data, therefore, demonstrate an indirect control of ice mass on GLOF magnitude in the catchment.

The Baker palaeodischarge record has implications for the geomorphology and ecohydrology of Pacific draining river basins and the fjords of Patagonia. These lake drainage events resulted in high sediment concentrations and large freshwater volumes (0.265–~100 km^3) delivered from glaciated areas to the ocean within short timescales. In the case of the catastrophic 0.1 Sv

Bertrand-Baker flood, Benito and Thorndycraft (2020) estimated a suspended sediment concentration (SSC) of up to 36 g/l at peak discharge producing locally a minimum sedimentation rate of 0.54 m/h. Such water and sediment flux would have produced short-term impacts in the fjord marine ecosystems by changing productivity, microbial activity and distribution of planktonic and benthic organisms (González et al., 2013). Marín et al. (2013) modelled the impacts of SSC produced by extreme GLOFs from the Baker valley on fjord hydrodynamics. They modelled three peak discharge scenarios within the range of our palaeodischarge reconstructions - 6000 m³/s, 9000 m³/s and 16,000 m³/s. According to Marín et al.'s (2013) findings, our flood data suggest that during GP-2 floods likely impacted light conditions and primary production in the outer channels and coastal waters. Light limitation during GP-3 would have reached the main fjords, while the fall in discharge by GP-5 (6000 m³/s) would have restricted the impacts on primary production to inner fjords.

6. Conclusion

The exceptional flood geomorphology of the Baker catchment makes it an ideal natural experimental setting to obtain long-term empirical palaeoflood data on glacier floods. Using a threshold discharge of 3500 m³/s, based on the modern instrumental data series, we determine a minimum of 86 palaeoflood GLOFs spanning the last 10,000 years allowing an evaluation of long-term flood magnitude and frequency in response to Holocene glacier dynamics. Our key findings are:

- We demonstrate that peak GLOF magnitude decreases through the Holocene from catastrophic floods of 0.1 Sv at the end of the Last Glacial Interglacial Transition, to events of 0.02–0.01 Sv during ~6.0–4.0 ka; 0.006 Sv at ~0.6 ka; and 0.004 Sv for modern floods of the instrumental period. This declining flood magnitude reflects an indirect control of ice-sheet mass.
- There is evidence for increased GLOF frequency at the end or post-dating three Holocene Patagonian neoglacials dated to 6–4 ka, 2–1 ka and 0.5–0.2 ka (Davies et al., 2020).
- Two well-developed palaeosols dated to ~7.0 ka and ~2.6 ka indicate periods of low flood frequency of high magnitude floods during ~10.0–7.0 ka and ~4.0–2.0 ka.
- The highest flood frequency in the record was at ~4.3 ka, with a phase of 26 floods of minimum discharges of 10,000–11,000 m³/s. These floods occurred at the end of the mid-Holocene (6–4 ka neoglacial), likely resulting from repeated ice-dam breaches during a phase of glacier instability.
- A Late Holocene phase of likely ice-dam failures caused at least 10 floods of 4600–5700 m³/s in magnitude at ~0.6 ka, while a possible moraine dam failure caused a flood of 5000–5600 m³/s at ~0.65–0.52 ka. These events post-dated the 2–1 ka neoglacial and pre-dated the 0.5–0.2 ka neoglacial.
- The modern instrumental GLOF series of peak discharges of 1000–3500 m³/s, while warranting an early warning flood system, are not exceptional in terms of flood magnitude in the context of the Baker valley composite GLOF record for the Holocene.

Author statement

G.B. and V.T. designed the study and wrote the first draft of the paper. G.B., V.T., C.S. and A.D. participated in the field data collection. G.B. and V.T. completed the palaeoflood stratigraphic descriptions and GLOF interpretations. GB conducted hydraulic modelling and flood discharge estimation, while V.T. undertook

interpretation of the compiled GLOF record in relation to Patagonian glacier ice mass changes. A.D. contributed to the hydrological analysis of modern floods. A.M. performed OSL sample preparation and numerical dating, and writing of the dating section. M.M. completed the soil and palaeosol descriptions, geochemical analysis and interpretation. All authors interpreted results, and contributed to paper editing.

Declaration of competing interest

The authors declare that they have no known competing financial interests or personal relationships that could have appeared to influence the work reported in this paper.

Acknowledgements

This paper is dedicated to the memory of Dr. Carlos Sancho, who died prematurely in February 2019. Carlos devoted his scientific career to Quaternary Science and palaeoclimate, and he was a source of inspiration to many colleagues and students. Fig. 7a shows a picture of Carlos (white cap) during stratigraphic descriptions of the Colonia reach during the field campaign in April 2011.

GB was supported by the Spanish Ministry of Science, Innovation and Universities. VT would like to thank the Natural Resources Defence Council and Royal Holloway University of London Research Strategy Fund (RHUL-RSF) for funding initial field visits that led to this research. AD thanks equipment and field support from CIEP, B. Reid, DGA-Aysén, J. Tureo, C. Meier, C. Olivares, H. Soto, M. Williams (U Greenwich) and NERC-GEF. Xavier Rodriguez-Lloveras provided field assistance during field work in April 2014. Giovanni Daneri (Centro de Investigación en Ecosistemas de la Patagonia, CIEP) provided logistical support for our field research.

References

Aniya, M., Naruse, R., 2001. Overview of glaciological project in Patagonia during 1998 and 1999: Holocene glacier variations and their mechanisms. *Bull. Glaciol. Res.* 18, 71–78.

Baker, V.R., 1973. Paleohydrology and sedimentology of Lake Missoula Flooding in eastern Washington. *Geological Society of America, Special Paper* 144, pp. 1–79.

Baker, V.R., 1987. Paleoflood hydrology and extraordinary flood events. *J. Hydrol.* 96, 79–99.

Baker, V.R., 2008. Paleoflood hydrology: origin, progress, prospects. *Geomorphology* 101, 1–13.

Baker, V.R., Kochel, R.C., 1988. Flood sedimentation in bedrock fluvial systems. In: Baker, V.R., Kochel, R.C., Patton, P.C. (Eds.), *Flood Geomorphology*. J. Wiley, New York, pp. 123–137.

Bendle, J.M., Palmer, A.P., Thorndycraft, V.R., Matthews, I.P., 2017a. High-resolution chronology for deglaciation of the Patagonian Ice Sheet at Lago Buenos Aires (46.5°S) revealed through varve chronology and bayesian age modelling. *Quat. Sci. Rev.* 177, 314–339.

Bendle, J.M., Thorndycraft, V.R., Palmer, A.P., 2017b. The glacial geomorphology of the Lago Buenos Aires and Lago Pueyrredón ice lobes of central Patagonia. *J. Maps* 13, 654–673.

Bendle, J.M., Palmer, A.P., Thorndycraft, V.R., Matthews, I.P., 2019. Phased Patagonian Ice Sheet response to southern Hemisphere atmospheric and oceanic warming between 18 and 17 ka. *Sci. Rep.* 9, 4133.

Benito, G., Thorndycraft, V.R., 2005. Palaeoflood hydrology and its role in applied hydrological sciences. *J. Hydrol.* 313, 3–15.

Benito, G., Thorndycraft, V.R., 2020. Catastrophic glacial-lake outburst flooding of the Patagonian Ice Sheet. *Earth Sci. Rev.* 200, 102996.

Benito, G., Sopena, A., Sanchez-Moya, Y., Machado, M.J., Perez-Gonzalez, A., 2003. Palaeoflood record of the Tagus River (Central Spain) during the Late Pleistocene and Holocene. *Quat. Sci. Rev.* 22, 1737–1756.

Caldenius, C.C.Z., 1932. *Las Glaciaciones Cuaternarias en la Patagonia y Tierra del Fuego*. Geogr. Ann. 14, 1–164.

Carrivick, J.L., 2006. Application of 2D hydrodynamic modelling to high-magnitude outburst floods: an example from Víkurfjöll, Iceland. *J. Hydrol.* 321, 187–199.

Carrivick, J.L., Quincey, D.J., 2014. Progressive increase in number and volume of ice-marginal lakes on the western margin of the Greenland Ice Sheet. *Global Planet. Change* 116, 156–163.

Carrivick, J.L., Tweed, F.S., 2016. A global assessment of the societal impacts of glacier outburst floods. *Global Planet. Change* 144, 1–16.

Carrivick, J.L., Turner, A.G., Russell, A.J., Ingeman-Nielsen, T., Yde, J.C., 2013. Outburst flood evolution at Russell Glacier, western Greenland: effects of a bedrock channel cascade with intermediary lakes. *Quat. Sci. Rev.* 67, 39–58.

Casanova, M., Salazar, O., Seguel, O., Luzio, W., 2013. The Soils of Chile, 1 ed. Springer Netherlands.

Chow, V.T., 1959. *Open-Channel Hydraulics*. McGraw-Hill, New York, p. 680.

Cook, K.L., Andermann, C., Gimbert, F., Adhikari, B.R., Hovius, N., 2018. Glacial lake outburst floods as drivers of fluvial erosion in the Himalaya. *Science* 362, 53–57.

Davies, B.J., Thorndycraft, V.R., Fabel, D., Martin, J.R.V., 2018. Asynchronous glacier dynamics during the Antarctic Cold Reversal in Central Patagonia. *Quat. Sci. Rev.* 200, 287–312.

Davies, B.J., Darvill, C.M., Lovell, H., Bindle, J.M., Dowdeswell, J.A., Fabel, D., García, J.-L., Geiger, A., Glasser, N.F., Gheorghiu, D.M., Harrison, S., Hein, A.S., Kaplan, M.R., Martin, J.R.V., Mendelova, M., Palmer, A., Pelto, M., Rodés, Á., Sagredo, E.A., Smedley, R.K., Smellie, J.L., Thorndycraft, V.R., 2020. The evolution of the Patagonian Ice Sheet from 35 ka to the present day (PATICE). *Earth Sci. Rev.* 204, 103152.

De La Cruz, R., Welkner, D., Suárez, M., Quiroz, D., 2004. Geología del área oriental de las hojas Cochrane y Villa O'Higgins, Región Aisén del General Carlos Ibáñez del Campo, escala 1:250.000. Serie Geología Básica, C.G.d.C., N° 85.. Servicio Nacional de Geología y Minería, Santiago, Chile.

Douglass, D.C., Singer, B.S., Kaplan, M.R., Mickelson, D.M., Caffee, M.W., 2006. Cosmogenic nuclide surface exposure dating of boulders on last-glacial and late-glacial moraines, Lago Buenos Aires, Argentina: interpretive strategies and paleoclimate implications. *Quat. Geochronol.* 1, 43–58.

Dubey, S., Goyal, M.K., 2020. Glacial lake outburst flood hazard, downstream impact, and risk over the Indian Himalayas. *Water Resour. Res.* 56, e2019WR026533.

Dussaillant, A., Benito, G., Buytaert, W., Carling, P., Meier, C., Espinoza, F., 2009. Repeated glacial-lake outburst floods in Patagonia: an increasing hazard? *Nat. Hazards* 54, 469–481.

Dussaillant, A., Buytaert, W., Meier, C., Espinoza, F., 2012. Hydrological regime of remote catchments with extreme gradients under accelerated change: the Baker Basin in Patagonia. *Hydrol. Sci. J.* 57, 1530–1542.

Flint, S.S., Prior, D.J., Agar, S.M., Turner, P., 1994. Stratigraphic and structural evolution of the Tertiary Cosmelli Basin and its relationship to the Chile triple junction. *J. Geol. Soc.* 151, 251–268.

Galbraith, R.F., Roberts, R.G., Laslett, G.M., Yoshida, H., Olley, J.M., 1999. Optical dating of single and multiple grains of quartz from Jinmium rock shelter, Northern Australia: Part I, experimental design and statistical models. *Archaeometry* 41, 339–364.

Glasser, N.F., Hambrey, M.J., Aniya, M., 2002. An advance of Soler Glacier, North Patagonian Icefield, at c. AD 1222–1342. *Holocene* 12, 113–120.

Glasser, N.F., Harrison, S., Schnabel, C., Fabel, D., Jansson, K.N., 2012. Younger Dryas and Early Holocene age glacier advances in Patagonia. *Quat. Sci. Rev.* 58, 7–17.

González, H.E., Castro, L.R., Daneri, G., Iriarte, J.L., Silva, N., Tapia, F., Teca, E., Vargas, C.A., 2013. Land–ocean gradient in haline stratification and its effects on plankton dynamics and trophic carbon fluxes in Chilean Patagonian fjords (47°–50°S). *Prog. Oceanogr.* 119, 32–47.

Gut, B., 2008. *Trees in Patagonia*. Springer, Basel.

Harrison, S., Winchester, V., 2000. Nineteenth- and twentieth-century glacier fluctuations and climatic implications in the Arco and Colonia valleys, Hielo Patagónico Norte, Chile. *Arctic Antarct. Alpine Res.* 32, 55–63.

Harrison, S., Glasser, N., Winchester, V., Haresign, E., Warren, C., Jansson, K., 2006. A glacial lake outburst flood associated with recent mountain glacier retreat, Patagonian Andes. *Holocene* 16, 611–620.

Harrison, S., Winchester, V., Glasser, N., 2007. The timing and nature of recession of outlet glaciers of Hielo Patagónico Norte, Chile, from their Neoglacial IV (Little Ice Age) maximum positions. *Global Planet. Change* 59, 67–78.

Harrison, S., Kargel, J.S., Huggel, C., Reynolds, J., Shugar, D.H., Betts, R.A., Emmer, A., Glasser, N., Haritashya, U.K., Klimeš, J., Reinhardt, L., Schaub, Y., Wiltshire, A., Regmi, D., Vilímek, V., 2018. Climate change and the global pattern of moraine-dammed glacial lake outburst floods. *Cryosphere* 12, 1195–1209.

Hein, A.S., Hulton, N.R.J., Dunai, T.J., Sugden, D.E., Kaplan, M.R., Xu, S., 2010. The chronology of the Last Glacial Maximum and deglacial events in central Argentine Patagonia. *Quat. Sci. Rev.* 29, 1212–1227.

Hervé, F., 1993. Paleozoic metamorphic complexes in the Andes of Aysén, southern Chile (West of Occidental). In: Ortega-Gutiérrez, F., Centeno-García, E., Morán-Zenteno, D.J., Gómez-Caballero, A. (Eds.), Circum-Atlantic Terrane Conference. Instituto de Geología, Universidad Autónoma de Mexico, Mexico City, Guanajuato, pp. 64–65.

Hogg, A.G., Heaton, T.J., Hua, Q., Palmer, J.G., Turney, C.S.M., Southon, J., Bayliss, A., Blackwell, P.G., Boswijk, G., Bronk Ramsey, C., Pearson, C., Petchey, F., Reimer, P., Reimer, R., Wacker, L., 2020. SHCal20 Southern Hemisphere calibration, 0–55,000 years cal BP. *Radiocarbon* 62, 1–20.

House, P.K., Pearthree, P.A., Klawon, J.E., 2002. Historical flood and paleoflood chronology of the Lower Verde River, Arizona: stratigraphic evidence and related uncertainties. In: House, P.K., Webb, R.H., Baker, V.R., Levish, D.R. (Eds.), *Ancient Floods, Modern Hazards: Principles and Applications of Paleoflood Hydrology*. American Geophysical Union, Washington, DC, pp. 267–293.

Hydrologic Engineering Center, 2010. *HEC-RAS, River Analysis System, Hydraulics Version 4.1*. Institute for Water Resources, U.S. Army Corps of Engineers, Davis, CA, p. 411.

Hydrologic Engineering Center, 2011. *HEC-GeoRAS – GIS tools for support of HEC-RAS using ArcGIS (v4.3/93), CPD-83*, February 2011. Institute for Water Resources, U.S. Army Corps of Engineers, Davis, CA User's Manual 244pp.

Iribarren Anacona, P., Norton, K.P., Mackintosh, A., 2014. Moraine-dammed lake failures in Patagonia and assessment of outburst susceptibility in the Baker Basin. *Nat. Hazards Earth Syst. Sci.* 14, 3243–3259.

Iribarren Anacona, P., Mackintosh, A., Norton, K., 2015. Reconstruction of a glacial lake outburst flood (GLOF) in the Engaño Valley, Chilean Patagonia: lessons for GLOF risk management. *Sci. Total Environ.* 527–528, 1–11.

Jacquet, J., McCoy, S.W., McGrath, D., Nimick, D.A., Fahey, M., O'kuhnghtons, J., Friesen, B.A., Leidich, J., 2017. Hydrologic and geomorphic changes resulting from episodic glacial lake outburst floods: Rio Colonia, Patagonia, Chile. *Geophys. Res. Lett.* 44, 854–864.

Kaplan, M.R., Strelin, J.A., Schaefer, J.M., Peltier, C., Martini, M.A., Flores, E., Winckler, G., Schwartz, R., 2020. Holocene glacier behavior around the northern Antarctic Peninsula and possible causes. *Earth Planet. Sci. Lett.* 534, 116077.

Kochel, R.C., Baker, V.R., 1982. Paleoflood hydrology. *Science* 215, 353–361.

Korup, O., 2012. Earth's portfolio of extreme sediment transport events. *Earth Sci. Rev.* 112, 115–125.

Loriaux, T., Casassa, G., 2013. Evolution of glacial lakes from the Northern Patagonia Icefield and terrestrial water storage in a sea-level rise context. *Global Planet. Change* 102, 33–40.

Marín, V.H., Tironi, A., Paredes, M.A., Contreras, M., 2013. Modeling suspended solids in a Northern Chilean Patagonia glacier-fed fjord: GLOF scenarios under climate change conditions. *Ecol. Model.* 264, 7–16.

Martin, J.R.V., Davies, B.J., Thorndycraft, V.R., 2019. Glacier dynamics during a phase of Late Quaternary warming in Patagonia reconstructed from sediment-landform associations. *Geomorphology* 337, 111–133.

Medialdea, A., Thomsen, K.J., Murray, A.S., Benito, G., 2014. Reliability of equivalent-dose determination and age-models in the OSL dating of historical and modern paleoflood sediments. *Quat. Geochronol.* 22, 11–24.

Meier, W.J.-H., Grießinger, J., Hochreuther, P., Braun, M.H., 2018. An updated multi-temporal glacier inventory for the Patagonian Andes with changes between the Little Ice Age and 2016. *Front. Earth Sci.* 6 (62), 1–21.

Mercer, J.H., 1976. Glacial history of southernmost South America. *Quat. Res.* 6, 125–166.

Niemeyer, H., Skarmeta, J., Fuenzalida, R., Espinoza, W., 1984. Hojas Península de Taitao y Puerto Aisén, Carta Geológica de Chile, N°60-61. Servicio Nacional de Geología y Minería, Santiago, Chile.

Nikiforoff, C.C., 1949. Weathering and soil evolution. *Soil Sci.* 67, 219–223.

Nimick, D.A., McGrath, D., Mahan, S.A., Friesen, B.A., Leidich, J., 2016. Latest Pleistocene and Holocene glacial events in the Colonia valley, Northern Patagonia Icefield, southern Chile. *J. Quat. Sci.* 31, 551–564.

O'Connor, J.E., Webb, R.H., 1988. Hydraulic modeling for paleoflood analysis. In: Baker, V.R., Kochel, R.C., Patton, P.C. (Eds.), *Flood Geomorphology*. John Wiley & Sons, United States, pp. 393–402.

Pfeiffer, M., Mascayano, C., Aburto, F., 2010. Soils of Chilean Patagonia in glacial and periglacial environments. *Eurasian Soil Sci.* 43, 1430–1438.

Prescott, J.R., Hutton, J.T., 1994. Cosmic ray contributions to dose rates for luminescence and ESR dating: large depths and long-term time variations. *Radiat. Meas.* 23, 497–500.

Ramsey, C.B., 2001. Development of the radiocarbon program OxCal. *Radiocarbon* 43, 355–363.

Retallack, G., 2001. *Soils of the Past*, second ed. Blackwell Science Ltd, London, p. 404.

Sagredo, E.A., Lowell, T.V., Kelly, M.A., Rupper, S., Aravena, J.C., Ward, D.J., Malone, A.G.O., 2016. Equilibrium line altitudes along the Andes during the Last millennium: paleoclimatic implications. *Holocene* 27, 1019–1033.

Sagredo, E., Kaplan, M., Araya, P., Lowell, T., Aravena, J., Moreno, P., Kelly, M., Schaefer, J., 2018. Trans-pacific glacial response to the Antarctic Cold Reversal in the southern mid-latitudes. *Quat. Sci. Rev.* 188, 160–166.

Snorrason, A., Jónsson, P., Sigurðsson, O., Pálsson, S., Árnason, S., Víkingsson, S., Kaldal, I., 2002. November 1996 jökulhlaup on Skeiðarársandur outwash plain, Iceland. In: Martini, P.I., Baker, R.V., Garzón, G. (Eds.), *Flood and Megaflood Processes and Deposits: Recent and Ancient Examples*. Wiley, pp. 55–65.

Soil Survey Staff, 2014. *Keys to Soil Taxonomy*, twelfth ed. USDA–Natural Resources Conservation Service, Washington, DC.

Tanaka, K., 1980. Geographic contribution to a periglacial study of the Hielo Patagónico Norte with special reference to the glacial outburst originated from glacier-dammed Lago Arco, Chilean Patagonia. *Centre Co Ltd, Tokyo*.

Thorndycraft, V.R., Benito, G., Rico, M., Sopena, A., Sanchez-Moya, Y., Casas, A., 2004. A Late Holocene paleoflood record from slackwater flood deposits of the Llobregat River, NE Spain. *J. Geol. Soc. India* 64, 549–559.

Thorndycraft, V.R., Bindle, J.M., Benito, G., Davies, B.J., Sancho, C., Palmer, A.P., Fabel, D., Medialdea, A., Martin, J.R.V., 2019. Glacial lake evolution and Atlantic-Pacific drainage reversals during deglaciation of the Patagonian Ice Sheet. *Quat. Sci. Rev.* 203, 102–127.

Tukey, J.W., 1977. *Exploratory Data Analysis*. Addison Wesley, Reading, Mass.

Turner, K.J., Fogwill, C.J., McCulloch, R.D., Sugden, D.E., 2005. Deglaciation of the eastern flank of the North Patagonian Icefield and associated continental-scale lake diversions. *Geogr. Ann. Phys. Geogr.* 87, 363–374.

Vandekerckhove, E., Bertrand, S., Mauquoy, D., McWethy, D., Reid, B., Stammen, S., Saunders, K.M., Torrejón, F., 2020. Neoglacial increase in high-magnitude glacial lake outburst flood frequency, upper Baker River, Chilean Patagonia (47°S). *Quat. Sci. Rev.* 248, 106572.

Villa-Martínez, R., Moreno, P., Valenzuela, M., 2012. Deglacial and postglacial vegetation changes on the eastern slopes of the central Patagonian Andes (47°S). *Quat. Sci. Rev.* 32, 86–99.

Walder, J.S., Costa, J.E., 1998. Outburst floods from glacier-dammed lakes: the effect of mode of lake drainage on flood magnitude. *Earth Surf. Process. Landforms* 21, 701–723.

Wilson, R., Glasser, N.F., Reynolds, J.M., Harrison, S., Anacona, P.I., Schaefer, M., Shannon, S., 2018. Glacial lakes of the Central and Patagonian Andes. *Global Planet. Change* 162, 275–291.

Winchester, V., Harrison, S., 2000. Dendrochronology and lichenometry: colonization, growth rates and dating of geomorphological events on the east side of the North Patagonian Icefield, Chile. *Geomorphology* 34, 181–194.